BRL

AD

CONTRACT REPORT NO. 328

SOME MEASUREMENTS OF THE MAGNUS CHARACTERISTICS ON A MAGNETICALLY-SUSPENDED 5-CALIBER OGIVE CYLINDER

Prepared by

MIT Aerophysics Laboratory
Cambridge, MA 02139

January 1977

USA BALLISTIC RESEARCH LABORATORIES
ABERDEEN PROVING GROUND, MARYLAND

Destroy this report when it is no longer needed.
Do not return it to the originator.

Secondary distribution of this report by originating or sponsoring activity is prohibited.

Additional copies of this report may be obtained from the National Technical Information Service, U.S. Department of Commerce, Springfield, Virginia 22151.

The findings in this report are not to be construed as an official Department of the Army position, unless so designated by other authorized documents.

The use of trade names or manufacturers' names in this report does not constitute indorsement of any commercial product.

REPORT DOCUMENTATION PAGE

READ INSTRUCTIONS BEFORE COMPLETING FORM

1. REPORT NUMBER: BRL Contract Report No. 328
2. GOVT ACCESSION NO.:
3. RECIPIENT'S CATALOG NUMBER:

4. TITLE (and Subtitle): SOME MEASUREMENTS OF THE MAGNUS CHARACTERISTICS ON A MAGNETICALLY-SUSPENDED 5-CALIBER OGIVE CYLINDER

5. TYPE OF REPORT & PERIOD COVERED: Final

6. PERFORMING ORG. REPORT NUMBER: MIT TR 193

7. AUTHOR(s): E. P. Birtwell, J. B. Coffin, E. E. Covert, and C. W. Haldeman

8. CONTRACT OR GRANT NUMBER(s): DAAD05-74-C-0735

9. PERFORMING ORGANIZATION NAME AND ADDRESS: MIT Aerophysics Laboratory, Cambridge, Massachusetts 02139

10. PROGRAM ELEMENT, PROJECT, TASK AREA & WORK UNIT NUMBERS: RDT&E 1L161102AH43

11. CONTROLLING OFFICE NAME AND ADDRESS: U.S. Army Ballistic Research Laboratory, Aberdeen Proving Ground, Maryland 21005

12. REPORT DATE: JANUARY 1977

13. NUMBER OF PAGES: 71

14. MONITORING AGENCY NAME & ADDRESS (if different from Controlling Office): U.S. Army Materiel Development & Readiness Cmd, 5001 Eisenhower Avenue, Alexandria, Virginia 22333

15. SECURITY CLASS. (of this report): Unclassified

15a. DECLASSIFICATION/DOWNGRADING SCHEDULE:

16. DISTRIBUTION STATEMENT (of this Report)

Approved for public release; distribution unlimited.

17. DISTRIBUTION STATEMENT (of the abstract entered in Block 20, if different from Report)

18. SUPPLEMENTARY NOTES

19. KEY WORDS (Continue on reverse side if necessary and identify by block number)

Magnus Force
Magnetic Balance
Subsonic Flow
Ogive Cylinder
Sting Effect

20. ABSTRACT (Continue on reverse side if necessary and identify by block number)

The Magnus side force and yawing moment on a spinning 5-caliber ogive cylinder have been measured using the magnetic suspension and balance system at the MIT Aerophysics Laboratory. Data are reported at M = .27 to .43 and Re = 1 x 10^5 to 1.2 x 10^6 at non-dimensional spin rate, PD/2V between 0 and 0.14. The Magnus side force is found to undergo reversal from its classical direction at angles of attack below 5° and Re = .77 x 10^6. Above 7° angle of attack the side force is in the classical direction and in agreement with the (Continued)

20. ABSTRACT (Continued):

data in the literature. The reverse Magnus force is a maximum at 2° angle of attack. The peak value is reduced by increase in Reynolds number, by artificially induced boundary layer transition and by the presence of a support sting. At angles of 7° and 9° both artificial roughness and a support sting increase the size of the classical Magnus force. Results are compared with other reported data.

TABLE OF CONTENTS

LIST OF FIGURES

LIST OF FIGURES (continued)

INTRODUCTION

It is probably no exaggeration to say that one of the older unsolved problems in fluid mechanics is a complete description of the Magnus characteristics of spinning bodies. This statement should not be taken to mean this problem has been ignored. On the contrary, three survey papers have been published in the last decade (1-3). As a result of this research the physics of the problem can be broadly explained under some circumstances. This is particularly true in the case of subsonic flow past a spinning two-dimensional cylinder whose spin axis (which is coincident with the axis of symmetry) is normal to the undisturbed velocity of the fluid. The data of Van Aken and Kelly (4) and of Swanson (5) qualitatively tends to support Krahn's (6) model for the variation of Magnus force with spin rate or velocity ratio (V/U). Krahn argues the Magnus force curve as a function of spin rate can have a negative region if the following conditions are satisfied. The boundary layer on the side of the cylinder moving in the same direction as the main flow is laminar. The boundary layer on the side of the cylinder moving against the free stream is turbulent. The negative region is due to the difference in the location of boundary layer separation in these two circumstances. Of course, transition and separation are more complicated than Krahn assumes, so his prediction of a sharp discontinuous change in the slope of the Magnus force

curve may not always occur. But a significant change in slope does occur and is more or less spread out, depending on the details of the separation of the laminar or turbulent boundary layers. Krahn's model, if extended, suggests the laminar side will become turbulent again after a suitable increase in V/U. The actual value of the increase suggested by data of Van Aken and Kelly or Swanson is of the order of 1/2 in V/U, which is larger than suggested by Krahn's model. Thus, not unexpectedly, the phenomena must be more complex than the simple model suggests. If this is the case in plane flow, the three-dimensional Magnus phenomena must be even more complicated and is explained in less detail.

Consider a three-dimensional flow. The main flow is more or less along the axis of symmetry of a slender body. This body is spinning about its axis of symmetry. The experimental data of Platou (7) and Platou and Nielson (8) show a strong influence of the base shape geometry on the Magnus forces. About this effect Jacobson (3) concludes "... In summary, it is evident that the Magnus force, moment and center of pressure are highly sensitive to anything which can have an effect on the boundary layer state or growth." This conclusion is particularly valid for intermediate range of Reynolds numbers.* For very large Reynolds numbers the potential model would seem to be

*The term intermediate range means the boundary layer on one side of the cylinder acts as if it were laminar, and on the other side the boundary layer acts as if it were turbulent.

adequate for large values of V/U, although the intercept of the force spin curve is incorrectly given unless one accounts for the offset in the velocity ratio. Fletcher (9) has used Krahn's idea, together with Swanson's data, to model the behavior when the cross-flow Reynolds number is in the transition range. If the angle of attack of the body is sufficiently large that the lift generated trailing vortex pair is identifiable, and if the separation point behavior is similar to that observed in cross-flow, and if certain experimentally-based approximations on the behavior of shed vorticity are made, Fletcher's model shows Magnus forces in the reverse direction. These results are surprisingly accurate in magnitude and extent of the reverse force region. These reverse forces also result from the difference between the angular point of "laminar separation" on one side of the body and the angular point of "turbulent separation" on the other. Both of these separated flows are represented by a potential flow model "with wake vortices". The terms in quotation marks are set off to remind the reader of two facts. One, separation in three-dimensional flow is much more complicated than in plane flow. These "separation" regions exhibit a well-organized axial flow. Two, the wake vortices are generally more closely related to Prandtl's lifting horseshoe vortices than the vortex flow behind a two-dimensional cylinder.

In supersonic flow the Magnus characteristics of finless bodies appear to be somewhat simpler in nature, particularly at higher angle of attack. There Inversen is able to make a reasonable correlation (Reference 3, Page 8). This is not true at small angles of attack where the state of the boundary layer seems again to be the dominant factor (Reference 3, Page 11).

Further, Regan and Schermerhorn's (10) base bleed experiment, while not producing data with a large change in Magnus characteristics, does support the contention that the flow is extremely complicated.

The conclusion from this short summary is neither new nor striking. Whatever the free-stream conditions, non-uniform behavior of the Magnus properties is to be expected when the spin ratio is of the order of one. This behavior results from a complicated, coupled interaction between the outer flow and the boundary layer flow.

In the material presented below additional experimental data taken on a magnetically-suspended model is presented that further supports the observation that the flow near the base has a profound effect on the Magnus characteristics. In fact, this data suggests Regan's statement that small "stings have virtually no effect on the data" should be used with caution, at least in the boundary layer transition regime, at low angles of attack.

DESCRIPTION OF THE EXPERIMENT

The experimental results described below are conducted at subsonic speeds, low enough in fact that compressibility can be neglected. The unique feature of the experiment is the model suspension system.. The model, a 5-caliber tangent ogive cylinder, is magnetically suspended. Thus, the aerodynamic interference between the suspension system and the model is negligible. The magnetic balance and suspension system has been described in detail elsewhere (11) as has the low-turbulence tunnel (12). This balance has been equipped with a laser angle of attack and angle of yaw measuring system to hold the angle of attack and yaw to the desired values within less than 0.02 degrees. This precision, as is well known, is needed to insure the Magnus force does not contain any component of normal force (13).

The model has a frontal blockage area of 2.25%. The length Reynolds number runs from 7×10^5 to 1.26×10^6. Thus, the boundary layer flow is in a transition region. Roughness was added to the surface to insure turbulent boundary layers in some cases. The spin rates or velocity ratios are of the order of 0.2 or less.

The model rolling motion was generated by superimposing a two-phase, 1200 Hz. A.C. electromagnetic field on the D.C. fields used for pitch and yaw control. A phase difference of 90 degrees between orthogonal components of the transverse

field induced the model to rotate about its longitudinal axis. To avoid spurious pickup by the control system caused by higher harmonics in the roll driving field, data was acquired as the model spin decayed from its peak value after the roll driving field was turned off.

Data Acquisition

Data output from the magnetic balance is read out as voltage signals from shunts in the several coil circuits. These signals for lift, side force, drag, pitch, yaw and magnetizing current are recorded with an integrating digital voltmeter (HP 2401C) and Digital recorder (HP 566-562A). During data readout the output signals are scanned sequentially by a United Systems "Digitec" Reed Relay Scanner.

In addition to balance force outputs, an output signal proportional to model spin was developed by a photocell, mounted in a transit, viewing ten black stripes painted longitudinally on the afterbody of the model. The frequency of the resulting signal from the photocell, counted for 0.1 second, gave the model spin rate in rps. Spin rate was recorded at the beginning and end of a data print cycle. The variation of spin rate was typically less than 3 rps over the two-second period of the scanning cycle.

Since the digital recorder required two seconds to print one set of ten numbers, the digital voltmeter was set to

integrate over a period of 0.1 second. The system would then measure and record one set of data points in two seconds. A timing device connected to the scanner prescribed this frequency of data gathering. During all Magnus testing data sets were recorded at eight-second intervals.

The pressure across the wind tunnel expansion section was measured with a micromanometer to 0.0003 psi and used to determine test section dynamic pressure. This reading was used to periodically check less accurate transducer readings which were printed with the other data.

Models

All three models used had the same external shape. This was a five caliber, tangent-ogive nose cylinder of one-inch base diameter. These were machined from electrolytic ingot iron and weighed approximately one pound each.

On two of the models different methods were employed to induce premature transition from a laminar boundary layer to a turbulent boundary layer. For the first method a thin layer of #180 carborundum grit was applied to the model nose. The grit started 1/4 inch from the tip of the nose and continued about one inch back. The other method used a single element device. In this case a thin (.012 inch) square ring of .57 inch diameter was slipped over the model nose and glued. The ring was .009 inches thicker than the boundary layer displacement thickness at its location to insure transition. The

two trip models, along with the bare model, are shown in Figure 1.

Drag vs. Reynolds number for nonspinning models at zero angle of attack is shown in Figure 2. The error bands are primarily due to errors in measuring "Q" at low Reynolds number. They get rapidly smaller as velocity is increased and are consistent with the error analysis given in Reference 14. The clean model boundary layer is in a boundary layer transition range above $Re = 6 \times 10^5$. Comparison of the drag coefficient curve with grit to the drag coefficient curve with the ring indicates the grit caused transition-to-turbulent boundary layer flow at lower Reynolds numbers. This is desirable so the grit "tripping" the boundary layer was used when a fully turbulent boundary layer was desired. Also shown in Figure 2 is an estimate of the drag coefficient following standard procedures (17). The results of the calculation are consistent with the interpretation of the data.

Dummy Sting Apparatus

In order to investigate the influence of a mounting sting on the Magnus force, a dummy sting was introduced immediately behind the magnetically-supported model. Because pylon-type sting supports were found to perturb the subsonic flow excessively, a wire-mounted* sting support was used.

*The authors wish to thank Mr. Anders S. Platou of the Army Ballistic Research Laboratory for his encouragement to conduct tests with this type of mounting.

The apparatus consists of a long sting holder, which accommodates three detachable front sections. Two of these are stings of .50 and .25 inch diameter (one half and one quarter of a caliber in this case), which extend from the holder to within 1/16 inch from the model base. The other is an ogive-nosed plug for streamlining the holder which leaves over six inches clearance to the model base. Each attachment is fitted with nylon screws for a tight fit into the holding device.

The sting-holding device is constrained in the diffuser by four .030 gauge piano wires. The wires pass through diametric holes bored through the holder where they are secured with set screws. By altering the tension in the various wires the position of the sting assembly can be adjusted.

The dummy sting apparatus is shown in Figure 3a. It is basically a streamlined cylinder having a length-to-diameter ratio of over 60, and a cross-sectional area of less than two percent that of the test section. The forward half of the apparatus is constructed of G-10 fiberglass (a nonmagnetic electrical insulator to insure no interference with the model position sensor). The rear half, located well into the diffuser, is aluminum, chosen as a nonmagnetic material with rigidity, durability and light weight. Interference of the sting holder alone on aerodynamic characteristics will be discussed below.

Testing Procedure

The magnetic balance equipment was turned on and permitted to stabilize with the model suspended for at least 15 minutes. The ambient air temperature and pressure were then recorded and the model position was adjusted to the desired location and angle of attack as measured by the position transits. The laser position control system was then locked on to hold the set angles of pitch and yaw. When drift in drag, lift and side slip position were observed through transits, zero position was adjusted using the position zero control.

Wind-off-tare balance currents were then recorded. The desired wind speed was set using the micromanometer. A wind on, zero-spin-tare was recorded. The model was spun using the roll field. When the spin rate, which was monitored on a separate electronic counter, reached its maximum (150-200 revolutions per second, depending on wind speed, angle of attack and boundary layer trip condition), the roll field was shut off allowing the spin to decay. The model position was held fixed during spin down, as data was recorded at eight-second intervals. The pressure transducer was used for all Magnus testing as a continuous measure of dynamic pressure, since micromanometer readings could not be read instantaneously. Micromanometer readings were recorded, however, at the beginning and end of each run for a calibration check. This procedure was followed for each condition tested.

All data was reduced on the IBM 370 at the M.I.T. Information Processing Center using the Magnus Data Reduction Computer Program (15). The output from this program is in the form of both print-out and punched cards. The punched cards were then used as input to a program that plotted aerodynamic coefficients vs. nondimensional spin rate ($PD/2V_\infty$) for each run.

Balance Calibration

The force current relations used for balance calibration are described in Reference 15. These were linearized for small angles of attack (16) and the seven calibration constants were determined by calibrations for each model tested.

To obtain the force and moment constants, loads were first applied to the model at the center of magnetization by the use of pulleys while the model was at zero angle of attack and angle of yaw. These loads were applied separately in lift, drag and side force. Then lift and side force loads were applied at different axial locations, producing pitching and yawing moments. The relationships between the applied forces and moments and the recorded coil currents then yielded the calibration constants. In this manner the calibration constants for lift, drag, side force, pitching moment and yawing moment were determined.

The pitching and yawing moment calibrations depend weakly on model angular position. Two additional constants are required to determine the angle/moment interaction in pitch and yaw (16). These constants were determined following the procedures of this reference.

TEST RESULTS

The results presented here include three series of experimental runs. Initially, Magnus measurements were made using the bare ogive-cylinder at small angles of attack. Subsequently, tests of the influence of stings and boundary layer trips were made (cf. Appendix A for the run schedule and test matrix).

During the initial testing period Magnus forces were measured on the bare model for spin rates up to 12,000 rpm, angles of attack from -5.5° to 9.5°, and at three wind speeds ranging from 300 to 460 ft/sec. Subsequent Magnus testing for the effect of stings and boundary layer trips was carried out at 300 ft/sec, as this was where the fullest extent of nonlinearity and Magnus reversal was observed. In the final test series the boundary layer tripped model was run at 400 ft/sec ($Re = 10^6$) to explore the changes caused by further increase in Reynolds number.

Measured Force and Moment Data

Force and moment data for all tests in the matrix detailed in Appendix A was reduced using the notation given in Appendix B. Figure 4 shows the normal force coefficient is weakly dependent on model spin. The measured side force and yawing moment coefficient, C_Y and C_N on a smooth model at three Reynolds numbers is shown as a function of nondimensional spin rate in Figures 5-8. Figures 5a to 8a indicate that the

Magnus force coefficient is generally nonlinear with spin and is not strongly dependent on Reynolds number at the highest angle of attack. The effect of Reynolds number becomes greater at lower angles of attack and is particularly important in the reversed Magnus regime (positive C_Y) at 2.5^o angle of attack. Similar comments may be offered for the Magnus moment coefficient (Figures 5b to 8b). The force and moment data suggest the center of pressure is essentially fixed. The summary plots, C_Y vs PD/2V curves from additional runs with a smooth sting free model are given in Figures 9 and 10. These curves at Re = $.77 \times 10^6$ show that the reverse Magnus force is very large at small angles of attack. It changes sign at about 4.5 degrees and then has the classical (negative) sign at higher angles of attack. Figure 11 shows the spin rate has little effect on the lift data.

The positive or reversed value of Magnus force and moment coefficient was an unexpected result. Thus, some additional tests were conducted to determine its origin. Two hypotheses were suggested. First the reverse loop could be eliminated with a sting. Second, it could be eliminated with a fully turbulent boundary layer, or both. The use of a sting required a support rig. Initially it was necessary to show the support rig has little or no effect on the data. The geometry of this equipment is shown in Figure 3a. The effect of the sting holder (with no sting) on C_Y is shown in Figure 3b. The sting holder has no measurable effect on C_Y.

Dummy stings in the sting holder do effect the Magnus side force and moment. This can be shown at Re = .77 x 10^6 as a function of spin rate by comparing the data in Figures 9 and 12. Note that the effect of the sting is to decrease the reverse Magnus force encountered at low spin rates. A cross plot vs. angle of attack at constant spin is shown in Figure 13 for no sting, .25 caliber sting and a .50 caliber sting. This clearly shows the effect of increasing sting diameter, which decreases the reverse Magnus force. Scatter in the data without sting at $\pm$ .5^o is a result of model jitter. The sting eliminates this jitter in model position, which is probably a result of the sting stabilizing the base flow. At higher angles of attack this data is consistent with Regan's claim (2) that stings have a negligible effect on Magnus data. Clearly this is not true at lower angles of attack.

The effect of a synthetic turbulent boundary layer with no dummy sting is shown by comparing the data in Figures 9 and 14a at Re = .77 x 10^6 and in Figure 14b at Re = 1 x 10^6. The reverse region is reduced when the dummy sting was installed behind a grit-roughened model and the reverse Magnus force is almost eliminated at small angles, as shown in Figure 15. Figure 16 shows these same data crossplotted vs. angle of attack at constant spin. At the highest Reynolds number tested (10^6), the sting and no sting data still show the same trend (Figure 17).

Comparison with Other Measurements

The amount of data to which this data can be compared is limited. Two references (18 and 19) have been found. The first comparison is the slope of the normal force coefficient curve and the slope of the pitching moment coefficient curve near zero angle of attack.

Source	C_{Z_α}	C_{M_α}	$\frac{*X_{CP}}{D}$	Re	M	Moment Ref
Greene	.040	.092	-	3.6×10^7	.23	"C.G." (unknown)
Platou	.042	-.0512	1.6	3×10^6	.11	nose
This data	.041	-.065	1.7	$.77 \times 10^6$	.27	"

The general agreement shown in the table is acceptable for normal force and center of pressure in diameters. The difference of 0.1 diameter on the center of pressure is at the limit of error for the data taken here (± 0.1 diameter). Platou's error bands are not listed. As explained below the error in C_Z is about ± 0.003 in the data obtained in the magnetic balance.

Figure 18 from Platou's report (19) shows a curve of C_{N_P}, the Magnus force parameter plotted against angle of attack. The Magnus center of pressure, in diameter from the nose, is also plotted against angle of attack. The filled symbols are data taken from Greene (18) while the open symbol represents

*Converted to a reference length of 1 diameter.

Platou's data. The center of pressure is in good agreement, while the size of the Magnus force coefficient, as determined by Greene, is about 0.1 times that determined by Platou. Platou's data corresponds to a Reynolds number of about 0.1 times Greene's data. Martin's theory suggests

$$C_{N_P} \alpha \frac{1}{\sqrt{Re}}$$

but this leaves Greene's data still too small by about one-third (or Platou's data too large by one-third). The latter is not believed to be the case since Platou's C_{N_P} is of the order of magnitude that is expected from Martin's theory.

Figure 19 shows the measured Magnus force coefficient plotted at a reduced spin of .045. It was assumed in getting these values that Platou's C_{N_P} curve could be linearly converted from his value of PD/2V at (0.4) to the value used here (0.045). This results in the values:

α	C_Y
2.5	.0013
5	.0031
7.5	.0077
10	.0122

which are plotted in Figure 19.

Except for the reversed loop the values from Reference 19 are in fair agreement with the data reported here, except they agree best with the data at Re = $.77 \times 10^6$ instead of 1.06×10^6 even though his data is taken at a Reynolds number of 1.15×10^6. However, difference in tunnel turbulence levels could easily account for this.

The center of pressure data is not well defined because of the small value of PD/2V. It seems to be at 4.5 diameters at 9.5 degrees, at 3.0 diameters at 2.5 degrees, again in fair agreement with the other data.

Error Analysis

A detailed review of the data indicate

$$\Delta C_X \simeq \pm .002 \qquad \Delta C_M \simeq \pm .015$$

$$\Delta C_Y \simeq \pm .01 \qquad \Delta C_N \simeq \pm .020$$

$$\Delta C_Z \simeq \pm .01 \qquad \Delta \alpha \simeq \pm .015 \text{ degrees}$$

The scatter in ΔC_N is unexpected, since usually it is comparable to ΔC_M. However, since C_N is about 0.1 of C_M, the difference may be due to a reduced signal-to-noise ratio.

The error in Magnus center of pressure (C.P.) is found from the formula

$$\frac{\Delta C.P.}{C.P.} = \frac{\sqrt{\Delta C_N^{\,2}}}{\left(\frac{C_N}{}\right)} + \left(C.P. \frac{\Delta C_Y}{C_Y}\right)^2$$

The results of using this formula are shown below:

	α	1.5	3.5	7.0	.95	
Magnus	$\frac{\Delta CP}{CP}$	2	8	1.6	.55	(diameter)

The large error at 3.5 is due to the small size of C_Y at that value of α. Corresponding results in pitch

Pitch	$\frac{\Delta CP}{CP}$	.650	.165	.100	.008	(diameter)

Hence the assertion that the primary source of error is in the smallness of the effect seems to be valid. Thus the data seems valid and accurate enough for detailed analysis.

DISCUSSION

Initially two points emerge from an examination of the data. As indicated above, in the laminar flow regime the reverse Magnus force exists at low angles of attack. The magnitude of the effect is larger, at a fixed reduced spin ($PD/2V_\infty$), as the Reynolds number is lower. The size of the Magnus force coefficient is larger as the Reynolds number is smaller. This Reynolds number sensitivity tends to be reduced to a negligible value at higher angles of attack. Comparing Figures 9 and 15 one sees the Magnus force coefficient on the model with forced transition is about twice that measured on a bare model. A detailed examination suggests the data of Figure 15 seems to be similar to that in Figure 9 except the curves are rotated counterclockwise until the slopes are doubled.

The forced transition case should result in a nearly axially symmetric locus. However, Sturek's data, References 21, 22 and 23, shows natural transition, which is not axially symmetric about the spin axis. No further discussion of this effect of artificial transition will be given since it has not been studied.

It has been suggested that one could approximate the aerodynamic characteristics of spinning bodies by the application of slender body theory (24).*

*That is if

$$S(x,\theta) = \int_0^{2\pi} \int_0^{r+\delta^*(\theta)} r \, dr \, d\theta$$

then one could compute the normal force. The angle of attack, α, is in radians

$$N = Q\,(2\alpha) \int_0^L dS(x)$$

the pitching moment with respect to the nose

$$M = Q\,(2\alpha) \int_0^L x\,dS(x)$$

Similarly, the side force or Magnus force

$$Y = Q \int_0^L \left(\left| \frac{d\delta^*}{dx} \right|_+ - \left| \frac{d\delta^*}{dx} \right|_- \right) dS(x)$$

and the Magnus moment with respect to the nose

$$N = Q \int_0^L x \left(\left| \frac{d\delta^*}{dx} \right|_+ - \left| \frac{d\delta^*}{dx} \right|_- \right) dS(x)$$

Here δ^* can be the laminar, turbulent or laminar and turbulent boundary layer displacement thickness.

However, slender body theory is a first order approximation. So it should be applied thoughtfully, if at all, to a second order problem.

The nature of the three-dimensional boundary layer helps to define the difficulty. It is driven externally by velocity components.

$$u_x = V_\infty \left(1 + \frac{2x-L}{x(L-x)} \frac{dS_0}{dx} - \ell n \left(\frac{4L(L-x)}{r^2}\right) - 2 \frac{d^2 S_0}{dx^2} + \ldots\right)$$

$$u_\theta = 2 V_\infty \sin \alpha \cos \theta$$

and internally by

$$u_\theta = Pr$$

Note $S_0 = \pi r^2$, where $r = r(x)$.

Thus the outer streamlines and wall streamlines are not confined to the same plane. All the complicated twist and curvature effects must be re-examined to determine their relative importance. Sturek's data shows some striking changes in the boundary layer transition location and in total head profiles for values of $PD/2V_\infty$ above 0.1. While one could possibly work backward and determine $\delta^* (\theta,x)$ to fit the integrated data, it is hard to see how a first order approximation could account for detailed changes in the flow pattern to produce the following observed facts:

1. The weak fractional increase in normal force due to spin.

2. The change in direction of the Magnus force in transition, without a large change in the center of pressure location, at least for the conditions of these tests.

3. The marked upstream influence of the "sting".

One concludes that if the boundary layer phenomena really dominates the flow, the test pattern should be run at constant spin and α and variable Re. This step would clarify the nature of the flow in the reversed sign part of Magnus curve, where if uneven transition is the dominant effect, one would expect migration in the center of pressure. At low spin rates in the range $0.06 < PD/2V < 0.05$ and at a Reynolds number of $.77 \times 10^6$ the Magnus side force behavior is peculiar (Figures 9 and 10). In this range the Magnus moment passes through zero. Figure 8b suggests this may be the region where more detailed studies of the transition from pathological Magnus force data to normal Magnus force data would be fruitful. There is a hint in Figure 7a at a Reynolds number of $.77 \times 10^6$ and PD/2V of .15 that this is the case. That is, the Magnus moment seems to be zero where there are changes in the sign of the Magnus force.

The success of the cross flow model in explaining the inverse sign Magnus force (9) at moderate angles of attack has been noted. Swanson's data (5) can be used to show this approximation is not valid in the small angle of attack range. In Figure 20 Swanson's data has been replotted in a relative spin ratio, Reynolds number plane with contours of constant Magnus force coefficient. Note the cross flow Reynolds number is

$$Re_c = Re_L \sin \alpha$$

and the corrected spin ratio is denoted $V/(U_\infty \sin \alpha)$ where α is the angle of attack. Thus at zero angle of attack $Re_c = 0$ and the relative spin is large without limit. As the angle of attack increases the path in the plane is traced out that moves toward smaller spin ratio and larger angle of attack. The path, therefore, does not initially fall in the inverse force range. Thus, the cross flow model seems to be incomplete or inadequate in this range (the low Reynolds number and high spin rate relative to the cross flow parameter).

Closing Remarks

This rather elementary experiment seems to have raised more issue than it settled. The well-defined but relatively small change in normal force with spin rate suggests the shed vorticity is altered more than enough to account for the Magnus force. In fact, the cross-force coefficient $\sqrt{(C_Z^2 + C_Y^2)}$ increases slightly with spin rate. Thus one expects that a detailed study of the interaction between the boundary layer vorticity on the one hand and the shed vorticity from the lift and spin on the other would be able to predict these results. Note, the data suggests the center of pressure is well behaved, even in the presence of the unexpected upstream influence of the sting, which seems strange indeed.

REFERENCES

1. Platou, A. S., "Magnus Characteristics of Finned and Unfinned Projectiles", AIAA Journal, Vol 3, No. 1, p 83-90, January, 1965.

2. Regan, F. J., "Magnus Effects" in AGARD CP 10; The Fluid Dynamic Aspects of Ballistics, September, 1966.

3. Jacobson, I. D., "Magnus Characteristics of Arbitrary Rotating Bodies", AGARDograph No. 171, November, 1973.

4. Van Aken, R. W., and H. R. Kelly, "The Magnus Force on Spinning Cylinders", Sherman M. Fairchild Publication Fund Preprint, No. 712 (AIAA copyright holder) (1957).

5. Swanson, W. M., "The Magnus Effect: A Summary of Investigations to Date", J Basic Engineering, pp 461-470, Sept 1961.

6. Krahn, E., "Negative Magnus Force", JAS, Vol 23, No. 4, p 377, April, 1956.

7. Platou, A. S., "The Magnus Force on a Short Body of Supersonic Speeds", BRL Report 1062, Aberdeen Proving Ground, Maryland, 1958. (AD #277353)

8. Platou, A. S. and G. I. T. Nielson, "Some Aerodynamic Characteristics of the Artillary Projectile XM 549", BRL Memo Rpt 2284, Aberdeen Proving Ground, Maryland, 1973. (AD #910093L)

9. Fletcher, C. A. J., "Negative Magnus Forces in the Critical Reynolds Number Regime", J. of Aircraft, Vol 9, No. 12, pp 826-833, December, 1972.

10. Regan, F. J. and V. L. Schermerhorn, "The Effect of Base Bleed on the Drag and Magnus Characteristics of a Rotating Body of Revolution", NOL TR 72-204, White Oak, Silver Spring, Maryland, August, 1972.

11. Covert, E. E., M. Vlajinac, T. Stephens and M. Finston, "Magnetic Suspension and Balance Systems for Wind Tunnel Use", Progress in Aerospace Science, Vol 14, Pergamon Press, London, 1973.

12. Vlajinac, M., "Design, Construction and Evaluation of a Subsonic Wind Tunnel", Thesis submitted to the Department of Aeronautics and Astronautics, M.I.T., for the S.M. degree, June, 1970.

13. Platou, A. S., "Wind Tunnel Magnus Testing of a Canted Fin on Self-Rotating Configuration", AIAA Journal, Vol 10, No. 7, pp 965-967, July, 1972.

14. Vlajinac, M. and E. E. Covert, "Sting Free Measurements of Sphere Drag in Laminar Flow", JFM 54, p 385, August, 1972.

15. Birtwell, E. P., "Magnus Forces and Sting Interference on Magnetically-Suspended Ogive Cylinders", Thesis submitted to the Department of Aeronautics and Astronautics, M.I.T. for S.M. Degree, May, 1974.

16. Gilliam, G. D., "Data Reduction Techniques for Use with a Wind Tunnel Magnetic Suspension and Balance System", NASA CR-111844, NaSl-8658, June, 1970 (also MIT Aerophysics Laboratory Report No. 162).

17. Hoerner, S. F., Fluid Dynamic Drag, 2nd Ed, Published by author, 1965.

18. Greene, J. E., "A Summary of Experimental Magnus Characteristics of a 7 and a 5-Caliber Body of Revolution at Subsonic through Supersonic Speeds", U.S. Naval Ordnance Laboratory (White Oak, Md), NAVORD, Report 6110 of 4 August 1958.

19. Platou, A. S., Edgewood Arsenal Magnus Tests, Unpublished, Ballistic Research Laboratory, Memorandum (AMXRD-BEL), U.S. Army Aberdeen Proving Ground (Md), April 29, 1971.

20. Carman, J. B., J. C. Uselton and W. E. Summers, "Experimental Magnus Characteristics of Basic and Boattail Configurations of 3- and 5-caliber Army-Navy Spinner Projectiles at Subsonic and Transonic Mach Numbers", AEDC-TR-70-36, April, 1970.

21. Sturek, W. B., "Boundary Layer Studies on Spinning Bodies of Revolution", BRL Memorandum Report 2381 (Aberdeen Proving Ground, Md), May, 1974. (AD #920069L)

22. Sturek, W. B., "Boundary Layer Studies on Spinning Tangent-Ogive-Cylinder Models", BRL Report 1801 (Aberdeen Proving Ground, Md), July, 1975. (AD #A014878)

23. Sturek, W. B., "Preliminary Surveys of the Three-Dimensional Boundary Layer on a Yawed, Spinning Body of Revolution", BRL Memorandum Report 2501 (Aberdeen Proving Ground, Md), July, 1975. (AD #B005829L)

24. Ashley, H. and M. Landahl, Aerodynamics of Wings and Bodies; Addison-Wesley Publishing Co., Inc., Reading, Ma., 1965, Chapt 6.7 for a discussion of the "Slender Body Approximation".

Figures

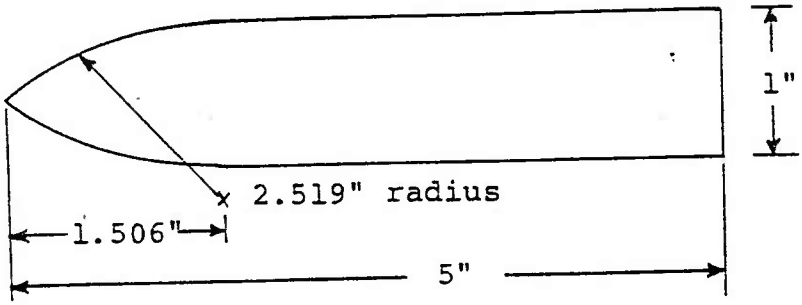

(a) Model Dimensions

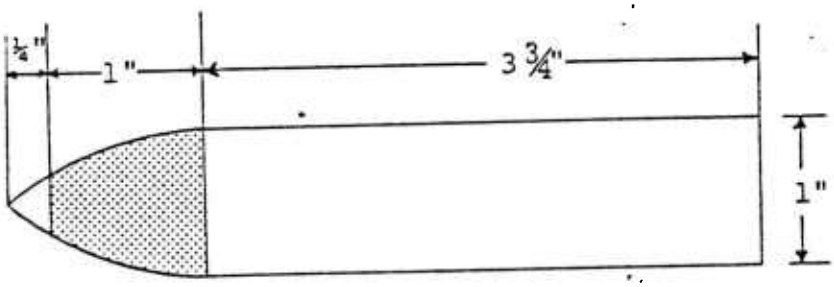

(b) Model with #180 Carborundum Grit

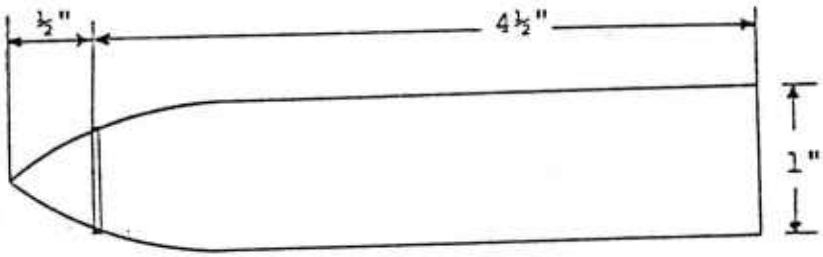

(c) Model with Trip Ring

Figure 1.

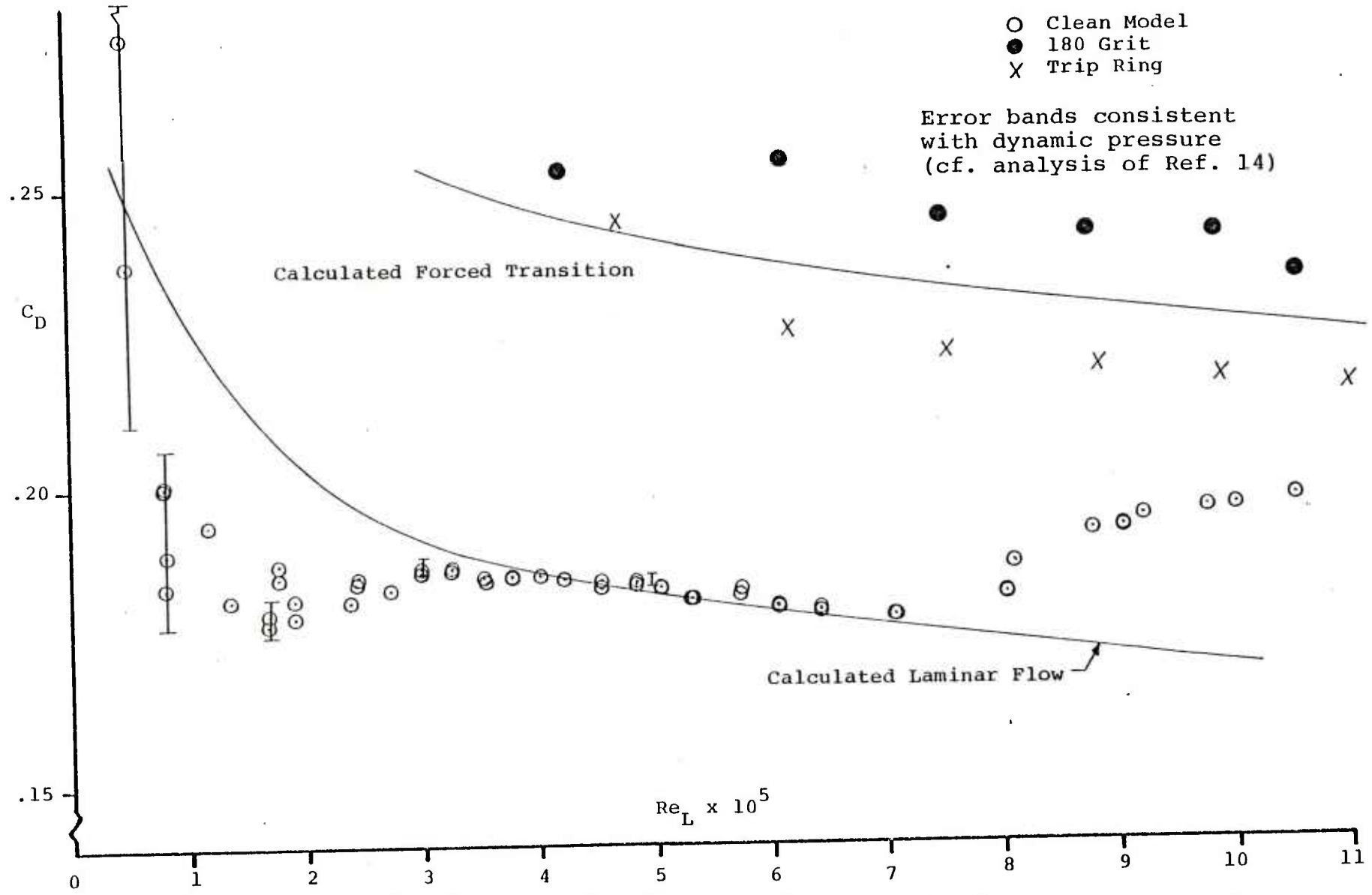

Figure 2. Drag Coefficient vs. Reynolds Number

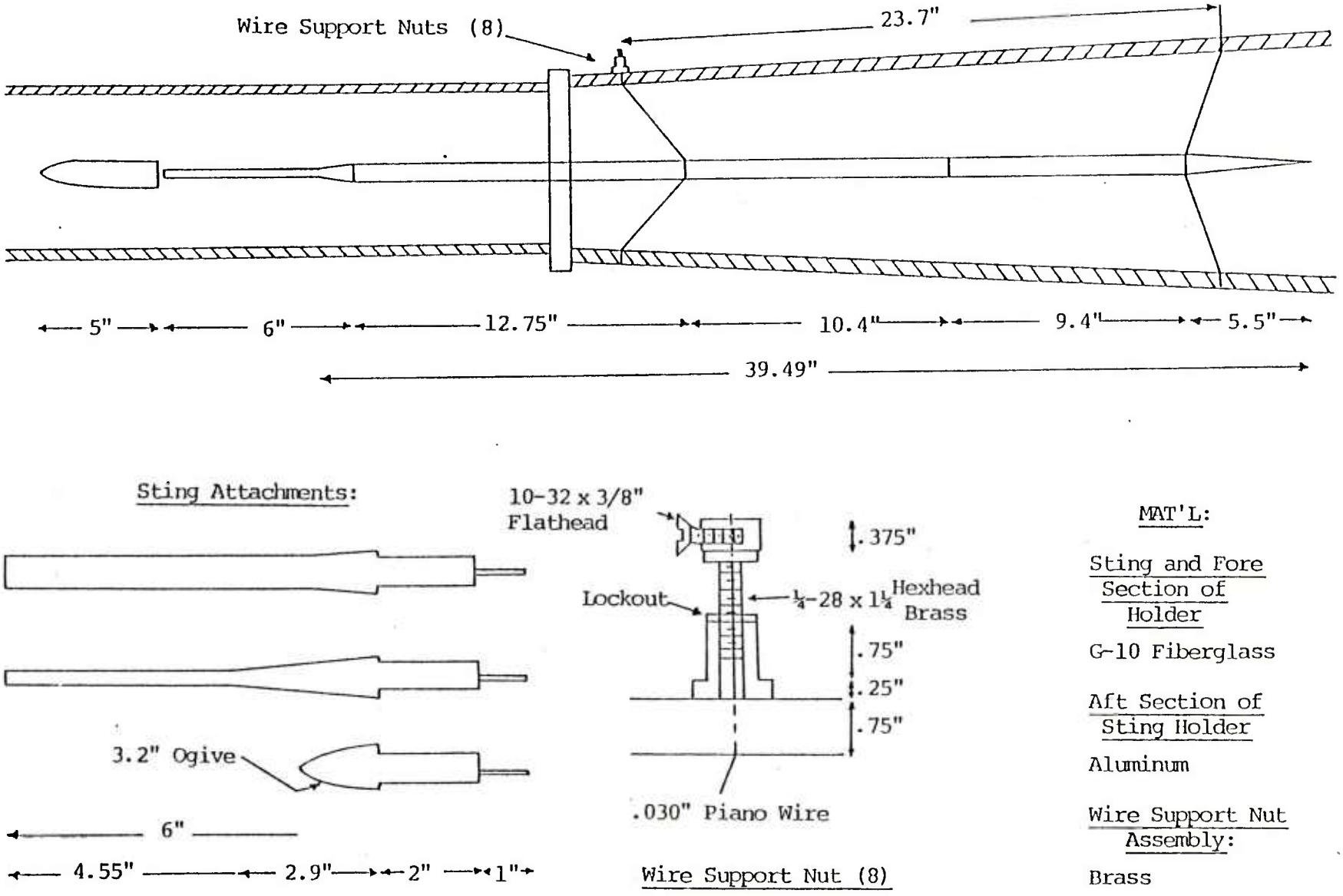

Figure 3a. Magnetic Balance Dummy Sting Assembly

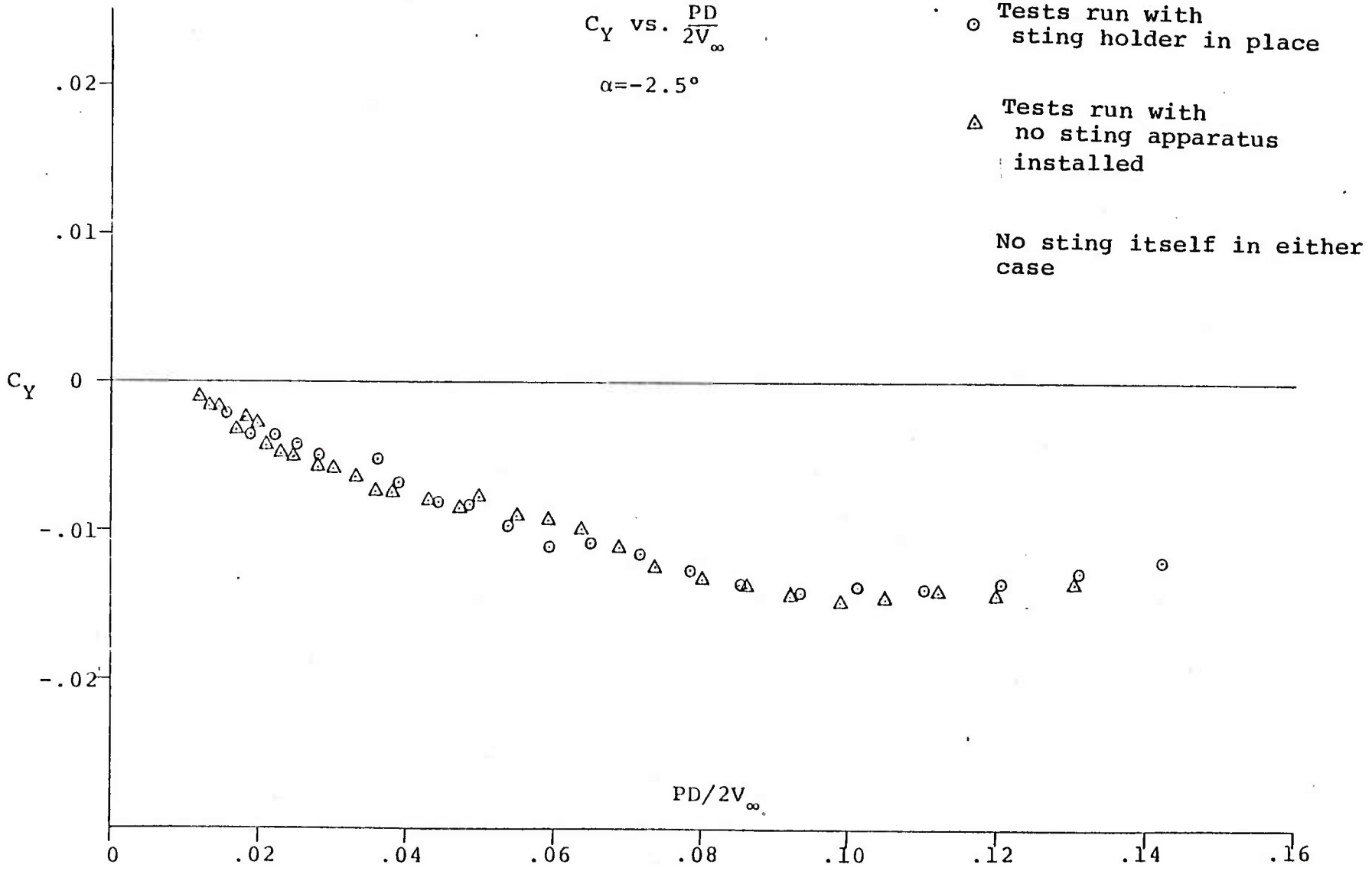

Figure 3b. Sting Holder Effect 5-1 Ogive Cylinder with no sting

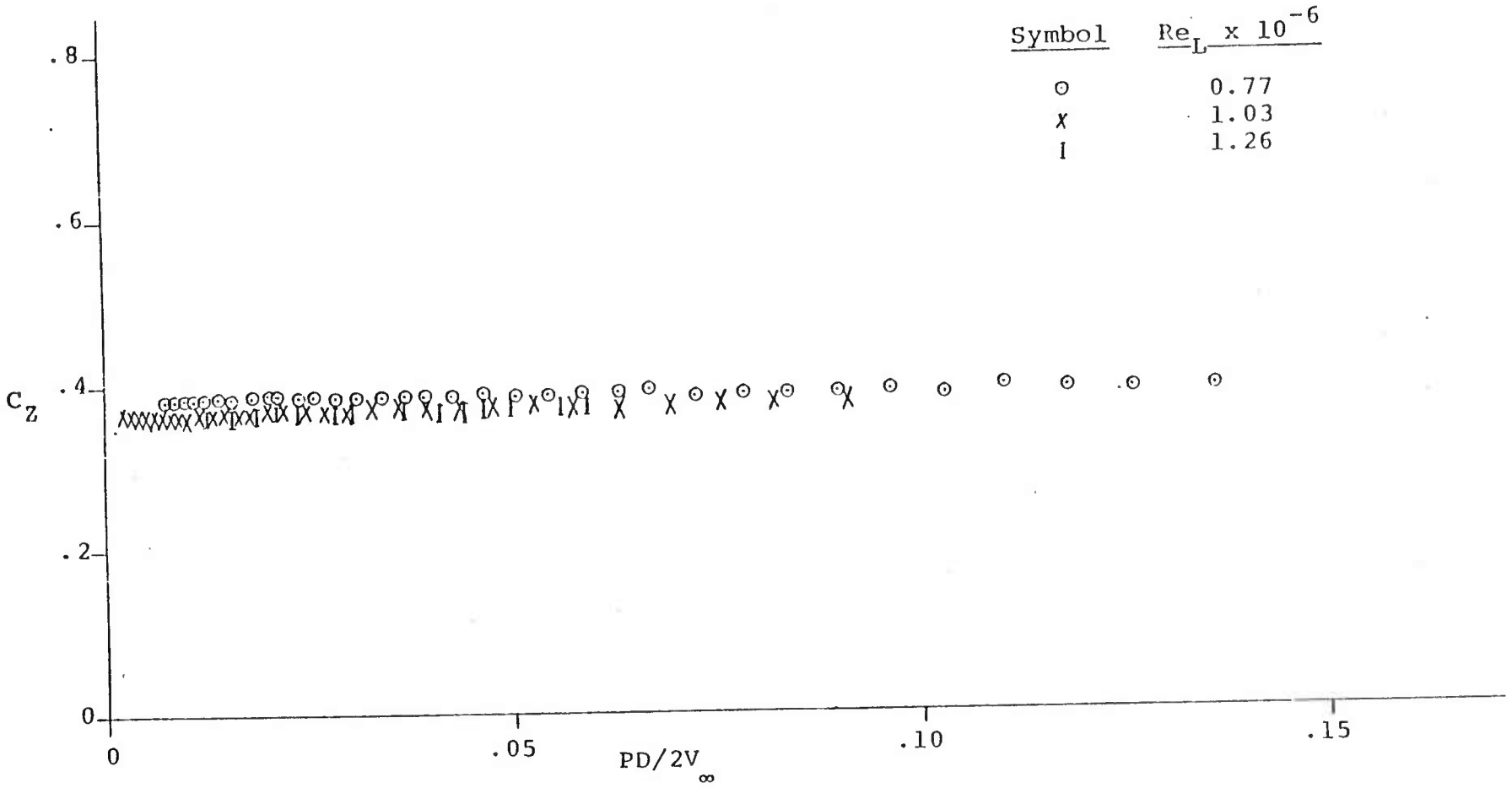

Figure 4. C_Z vs. $PD/2V_\infty$; $\alpha = 8.5^\circ$

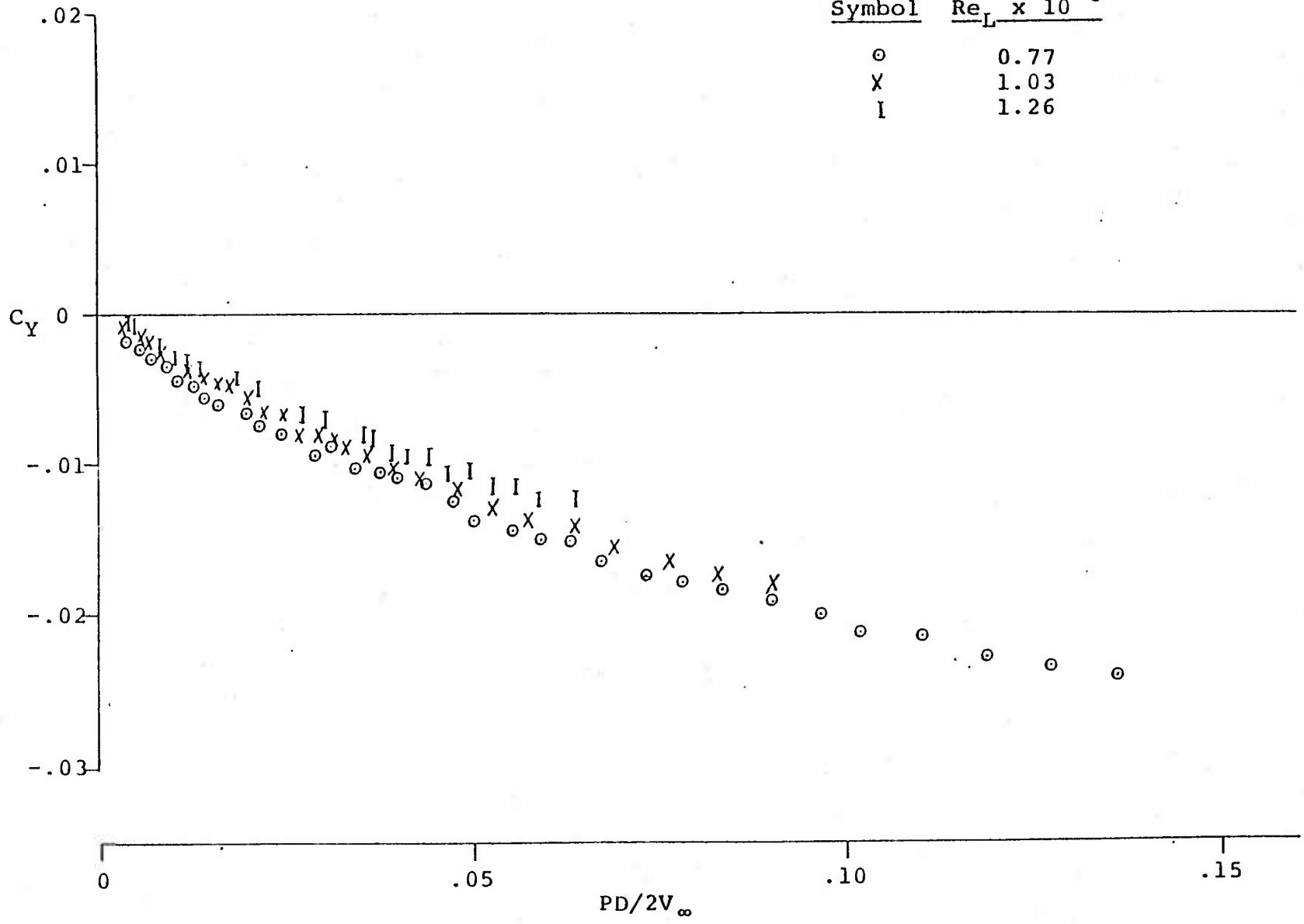

Figure 5a. Reynolds Number Effect C_Y vs. $PD/2V_\infty$; $\alpha = 9.5^o$

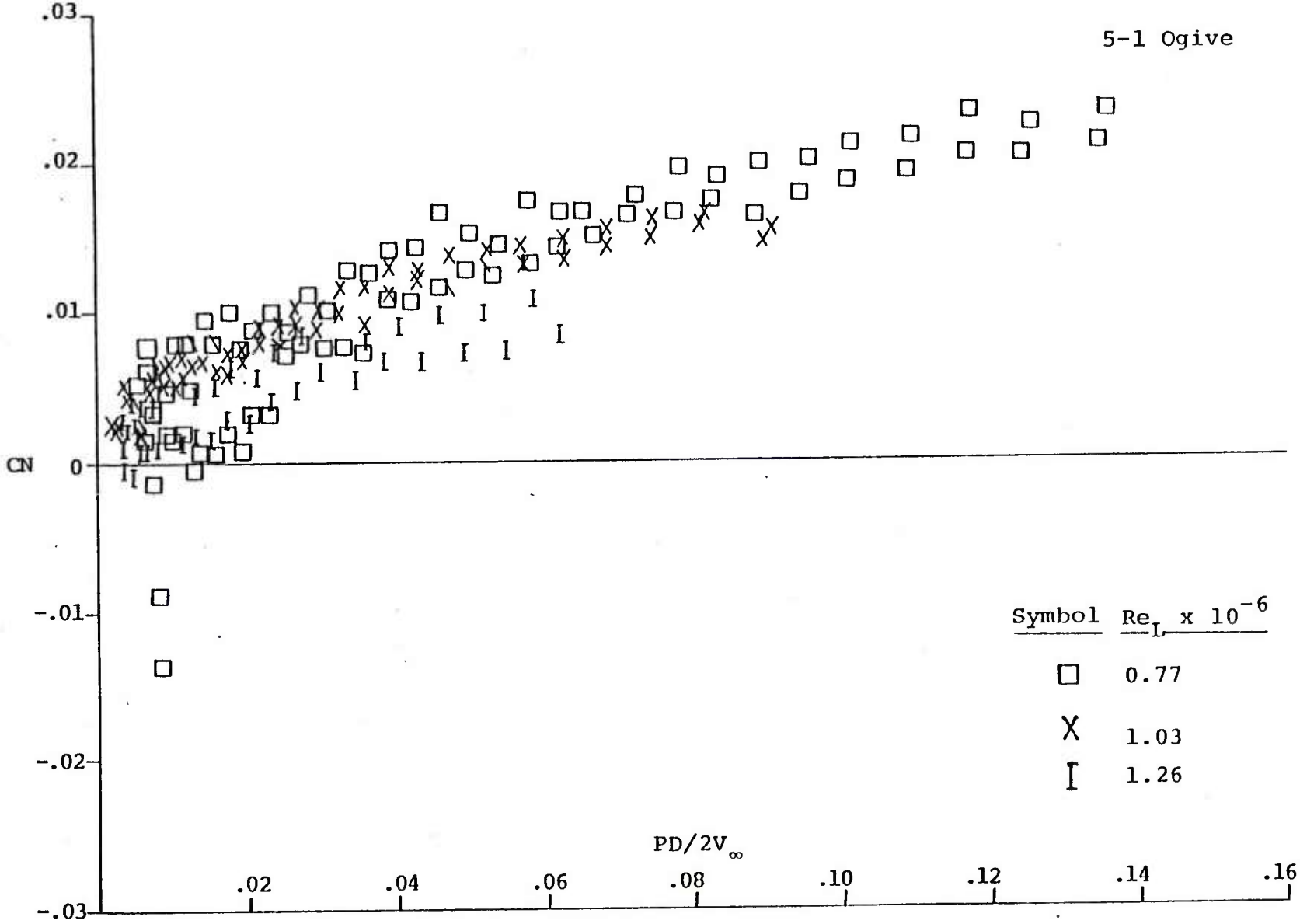

Figure 5b. Yawing Moment Coefficient; $\alpha = 9.5^{o}$

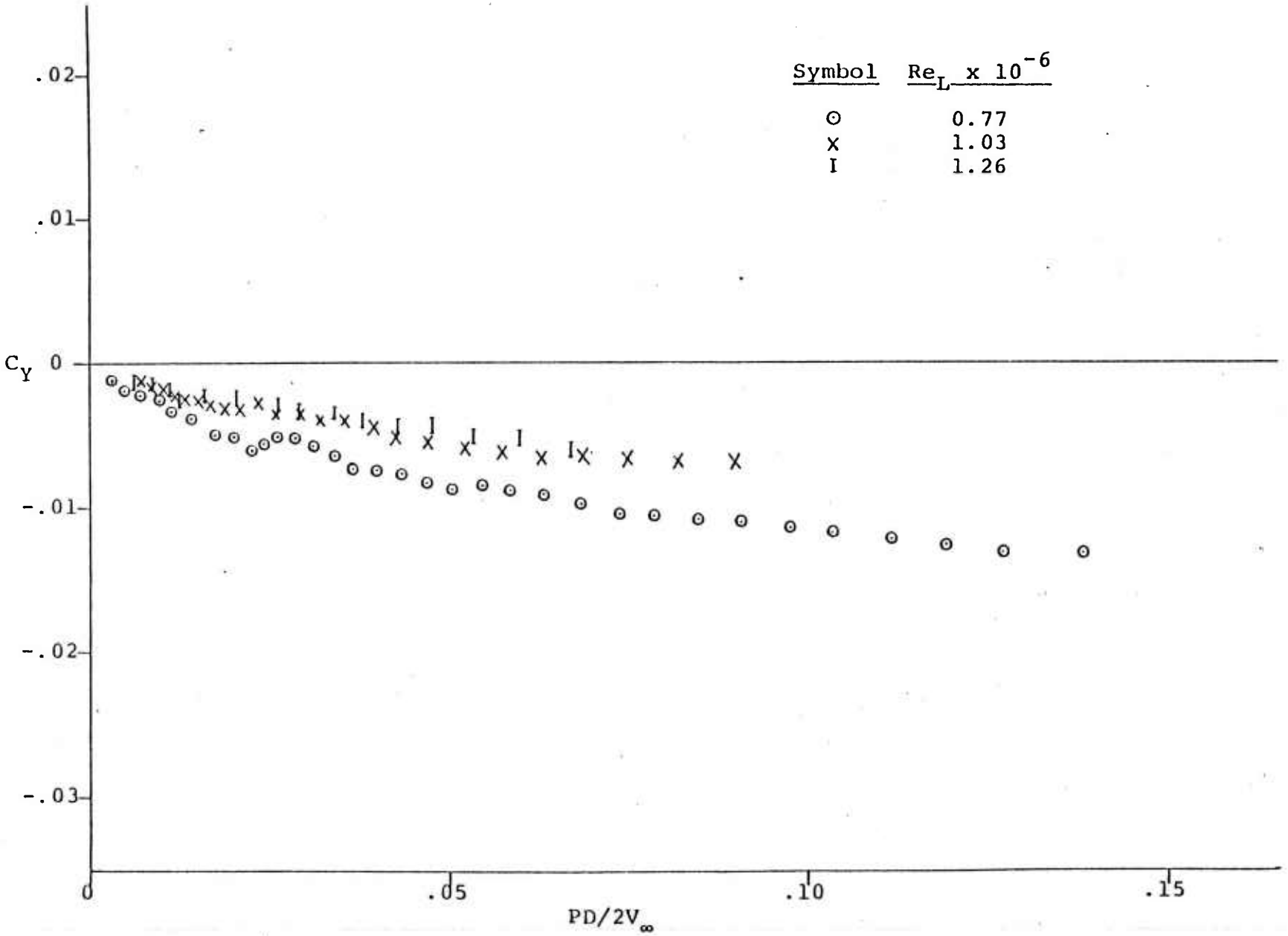

Figure 6a. Reynolds Number Effect C_Y vs. $PD/2V_\infty$; $\alpha = 7.0^\circ$

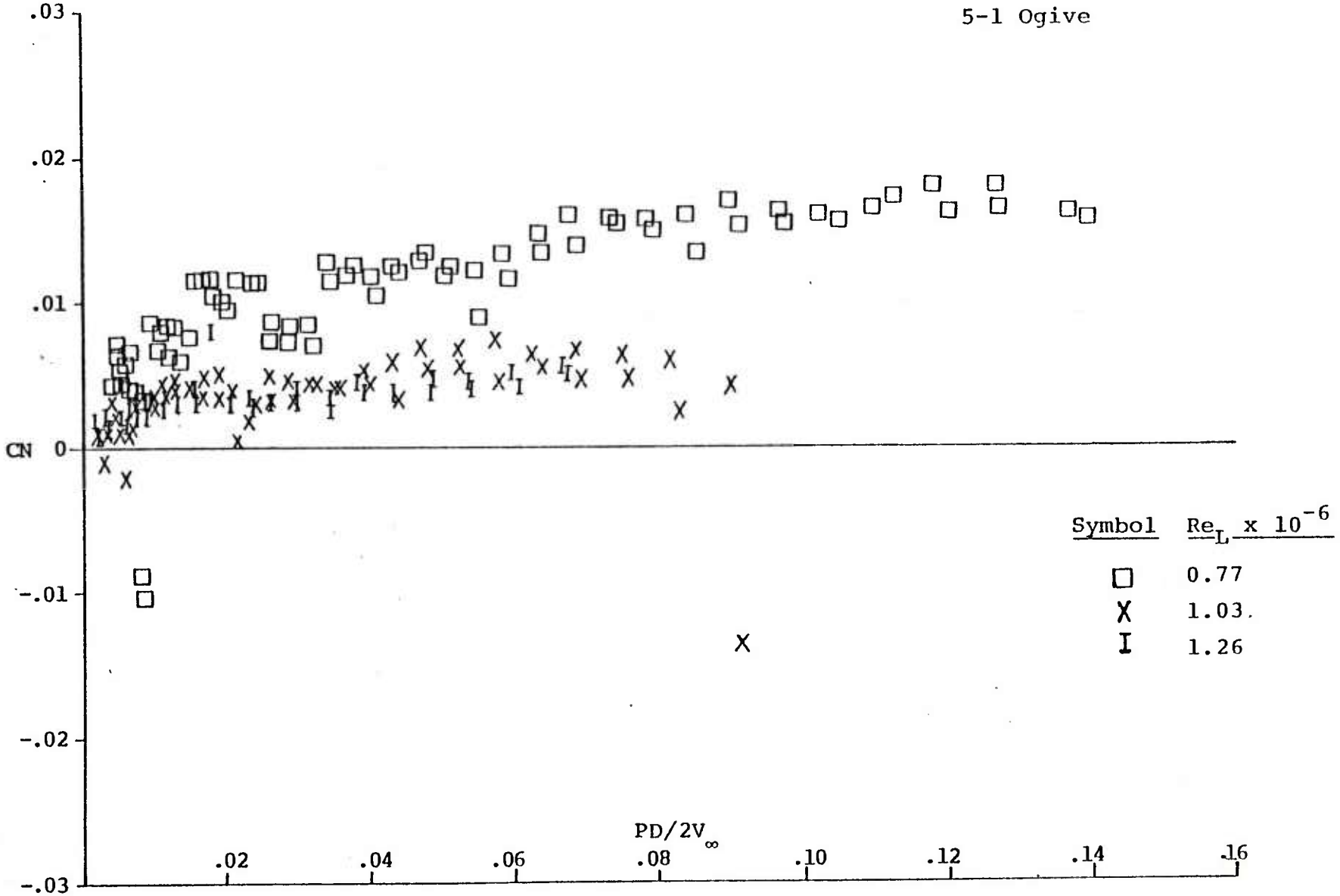

Figure 6b. Yawing Moment Coefficient; $\alpha = 7.0^{o}$

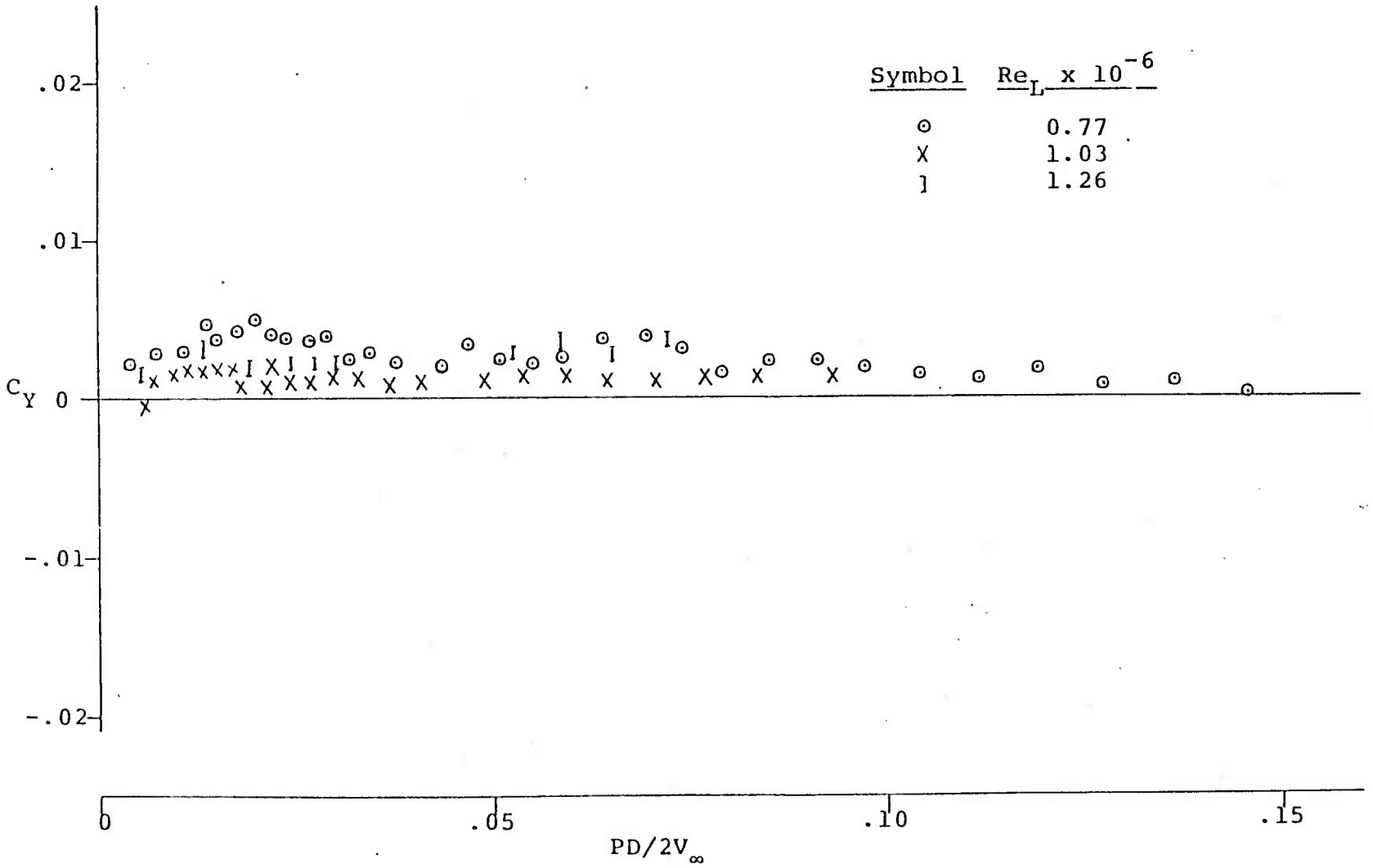

Figure 7a. Reynolds Number Effect C_Y vs. $PD/2V_\infty$; $\alpha = 4.5^O$

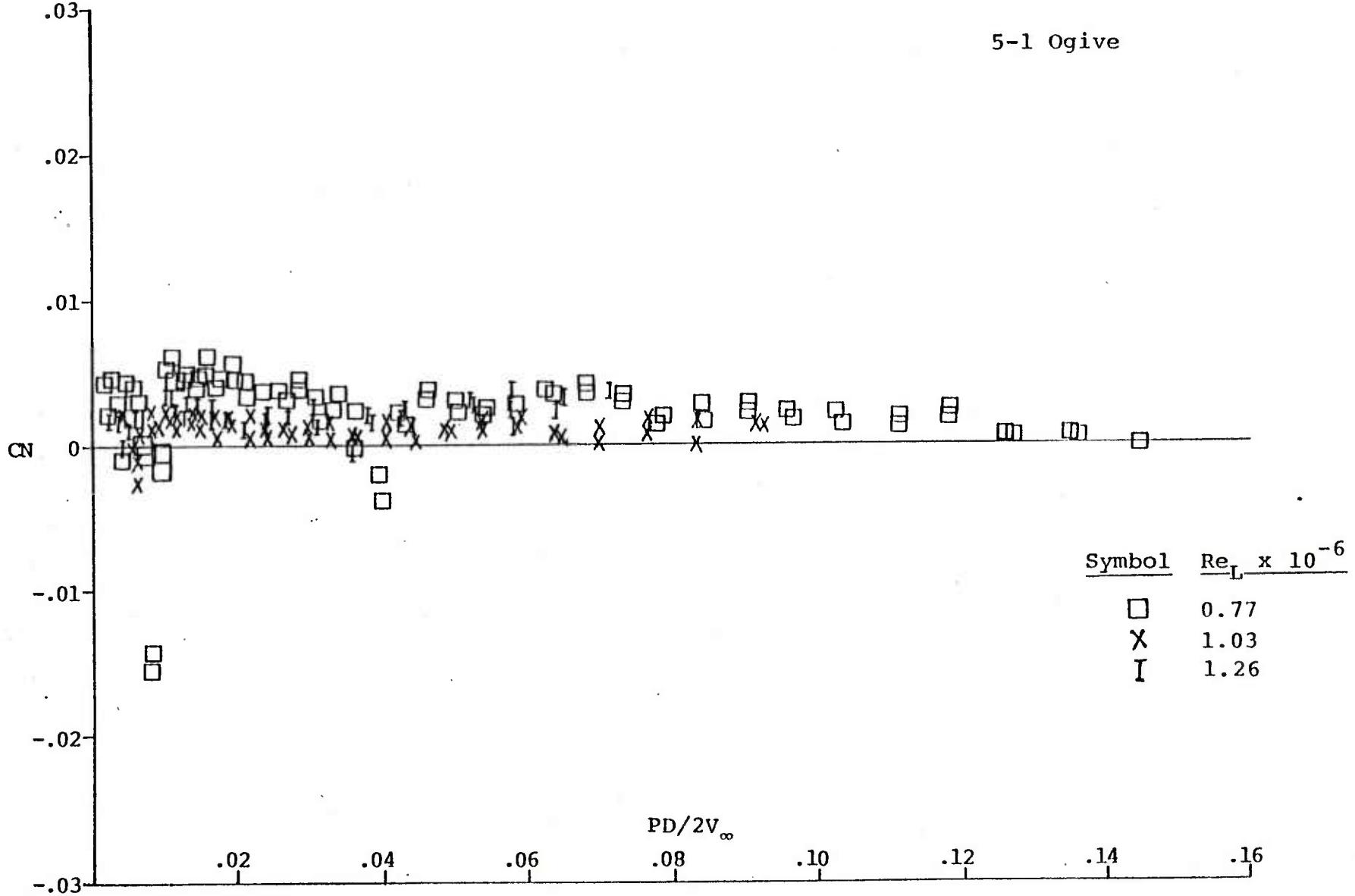

Figure 7b. Yawing Moment Coefficient; $\alpha = 4.5^{o}$

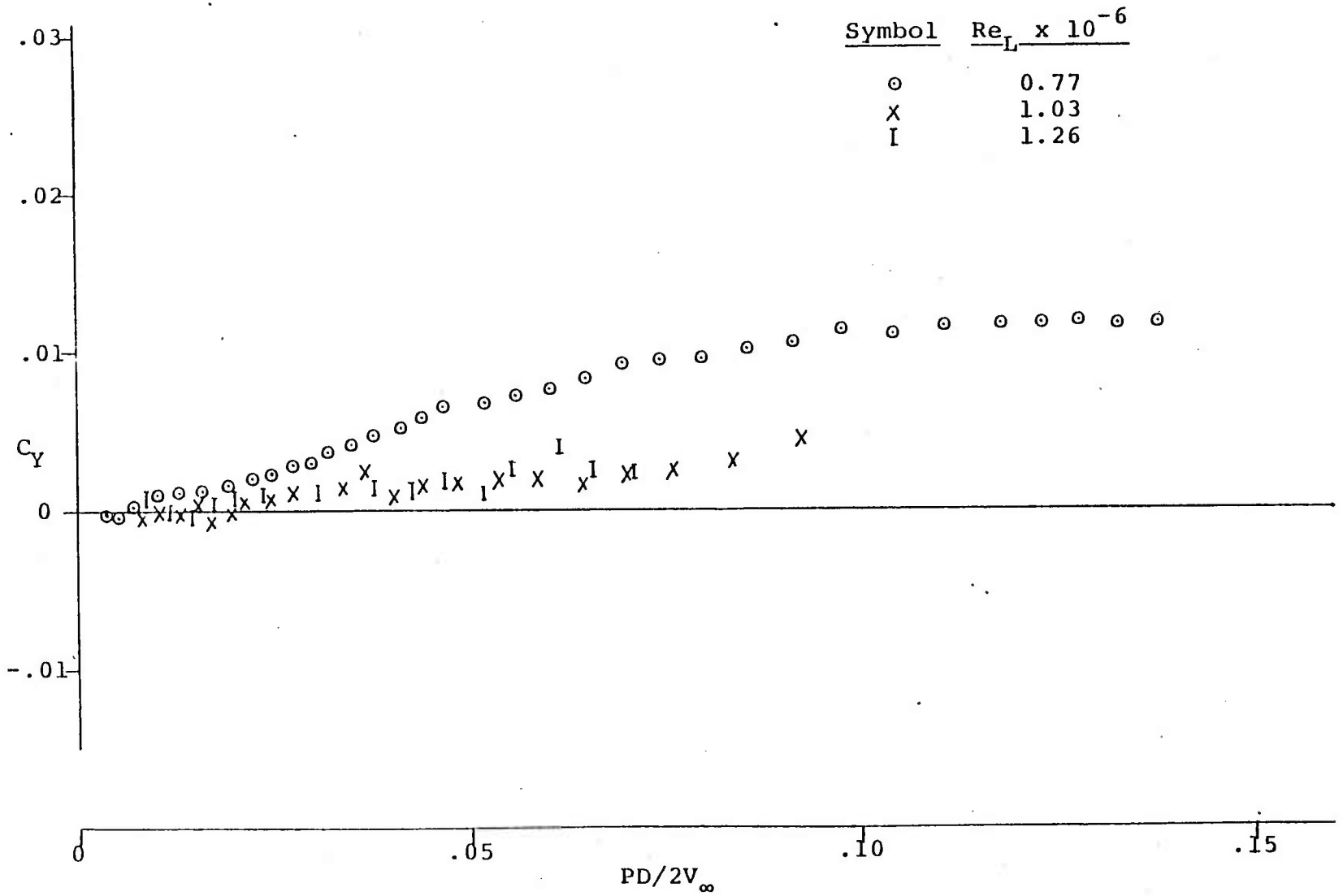

Figure 8a. Reynolds Number Effect C_Y vs. $PD/2V_\infty$; $\alpha = 2.5^O$

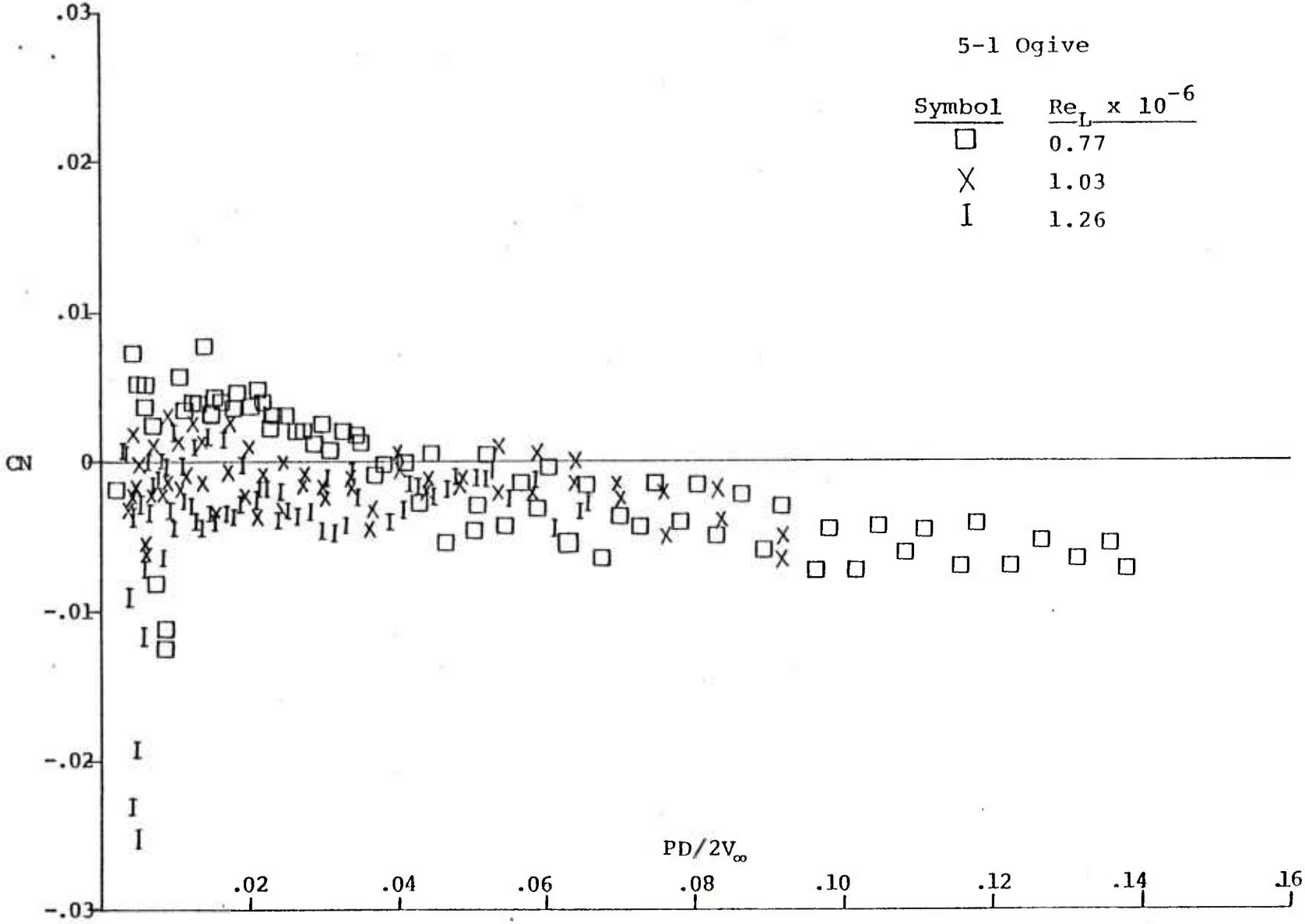

Figure 8b. Yawing Moment Coefficient; $\alpha = 2.5^{o}$

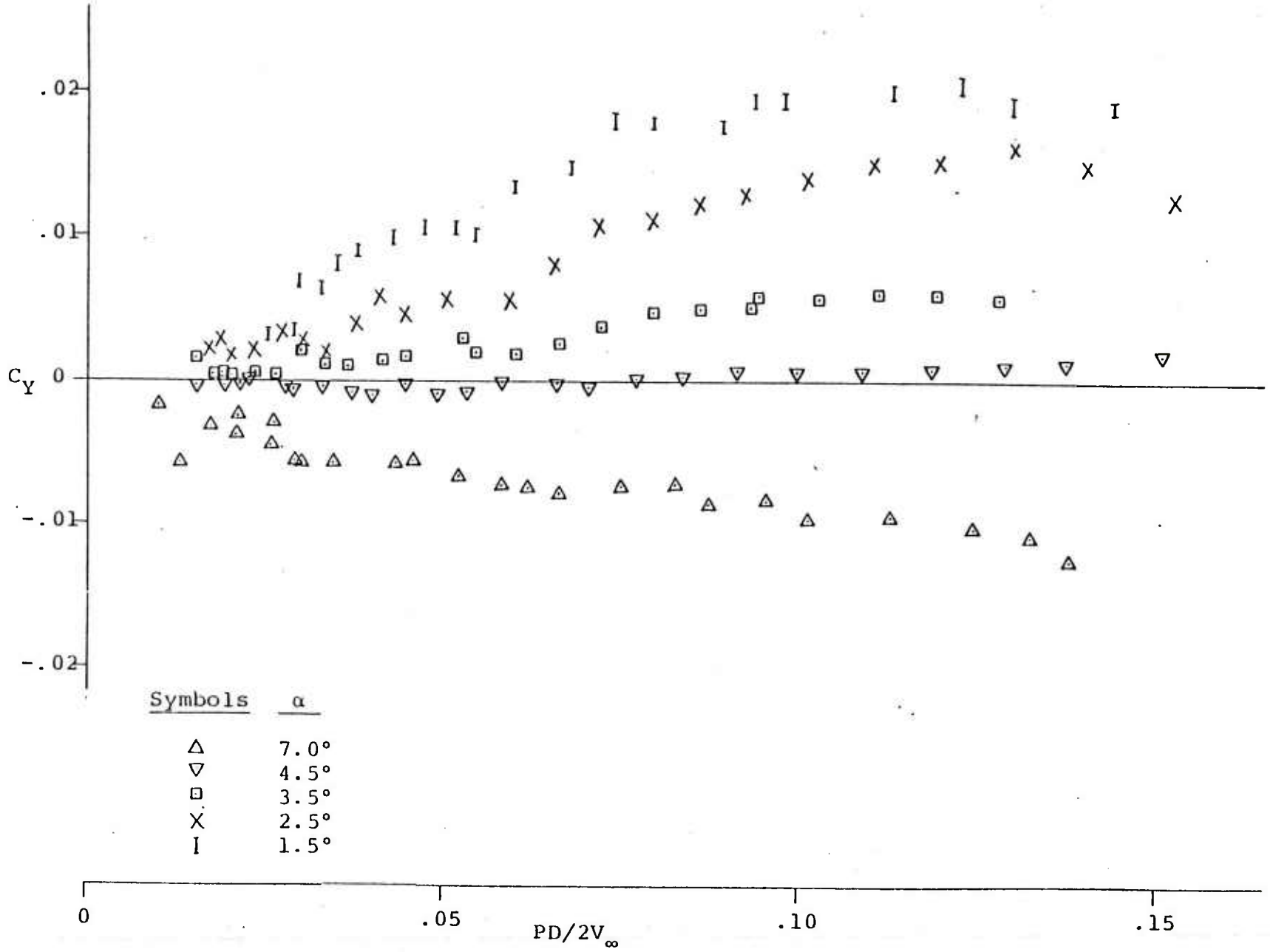

Figure 9. Bare Model C_Y vs. $PD/2V_\infty$ at $Re_L = .77 \times 10^6$

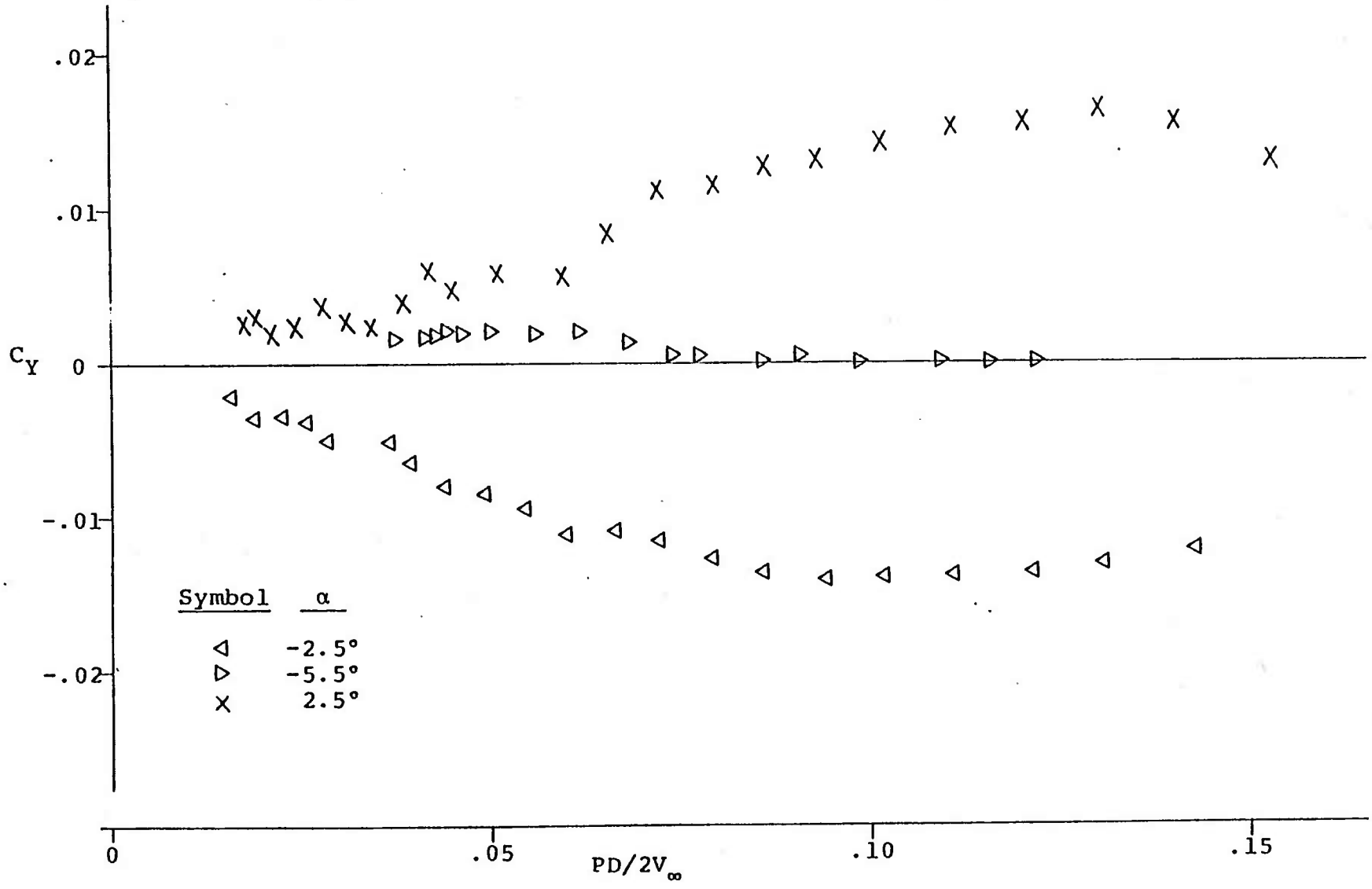

Figure 10. Bare Model C_Y vs. $PD/2V_\infty$ at $Re_L = .77 \times 10^6$

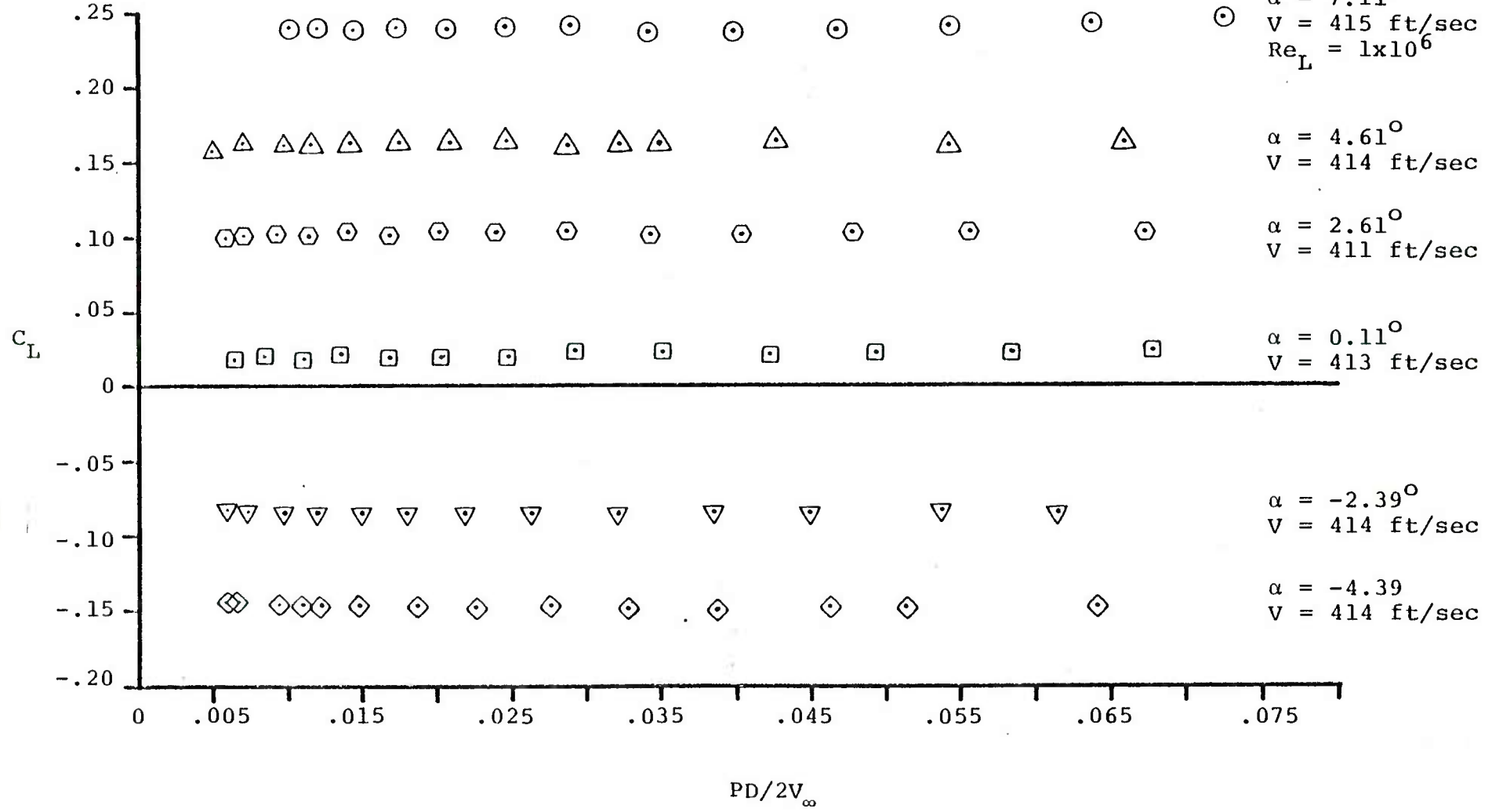

Figure 11. Lift Coefficient vs. $PD/2V_\infty$ (with grit)

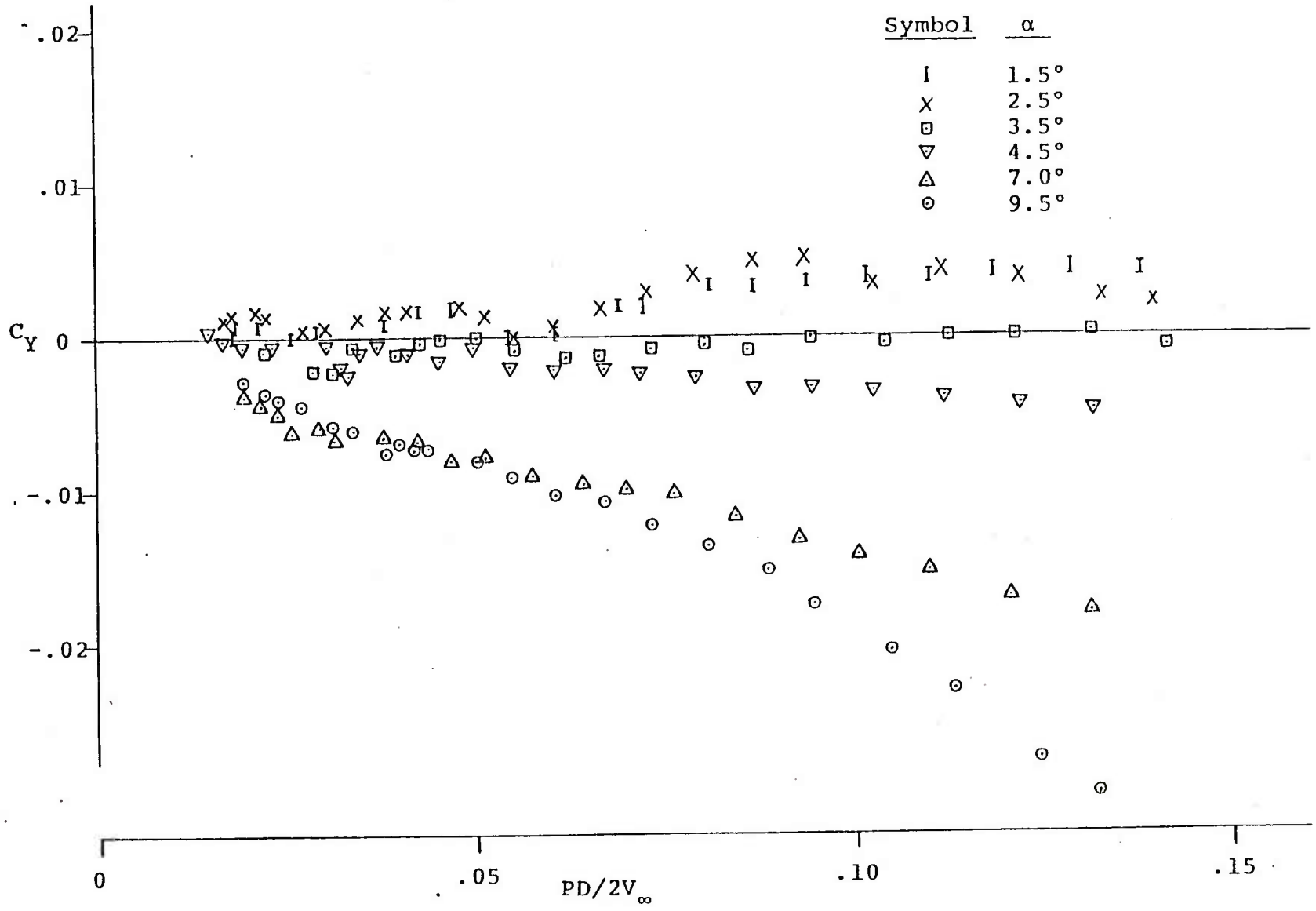

Figure 12. Model with .50 Caliber Sting C_Y vs. $PD/2V_\infty$ at $Re_L = .77 \times 10^6$

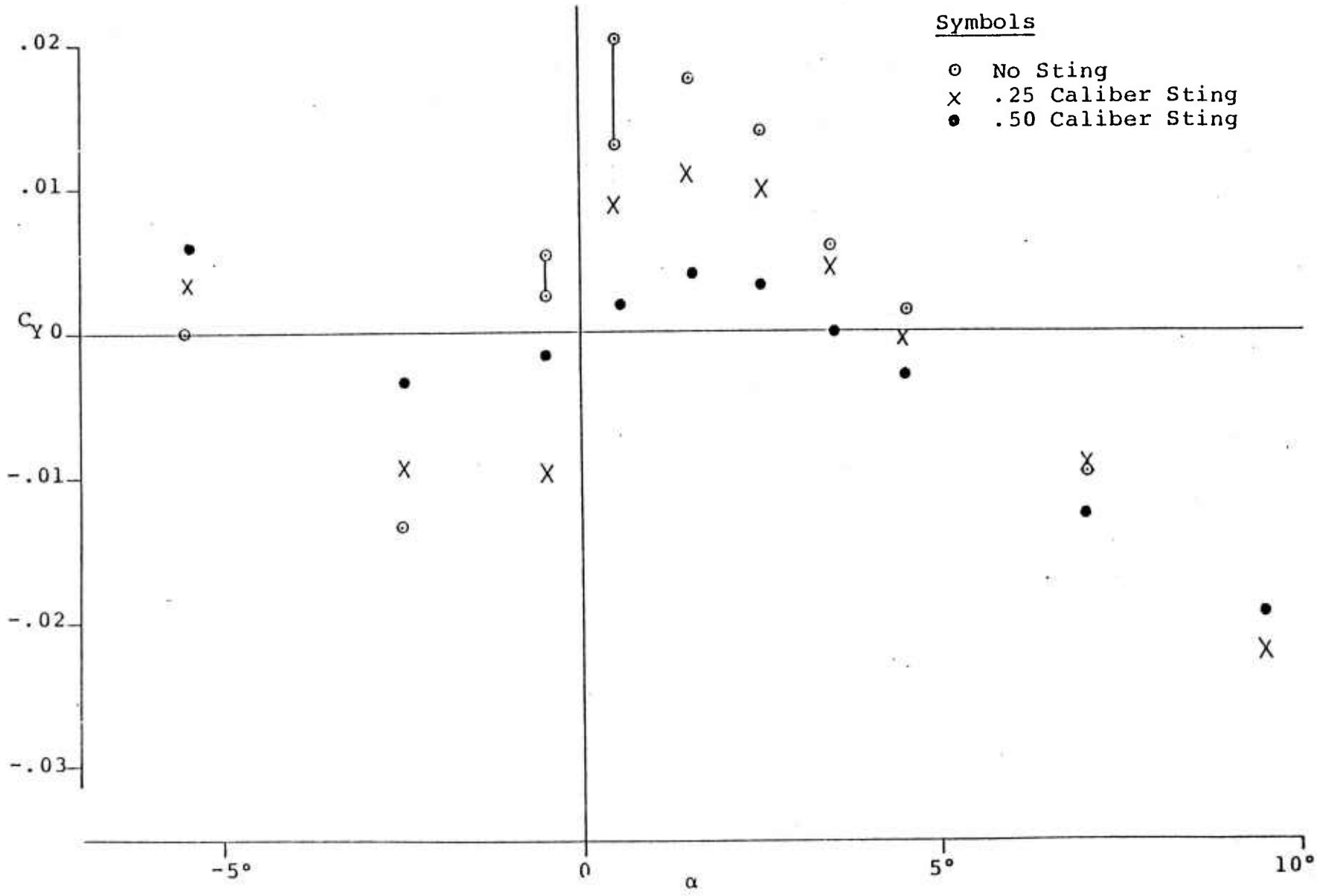

Figure 13. Sting Effect C_Y vs. $PD/2V_\infty$; $\alpha = 0.1$ at $Re_L = .77 \times 10^6$

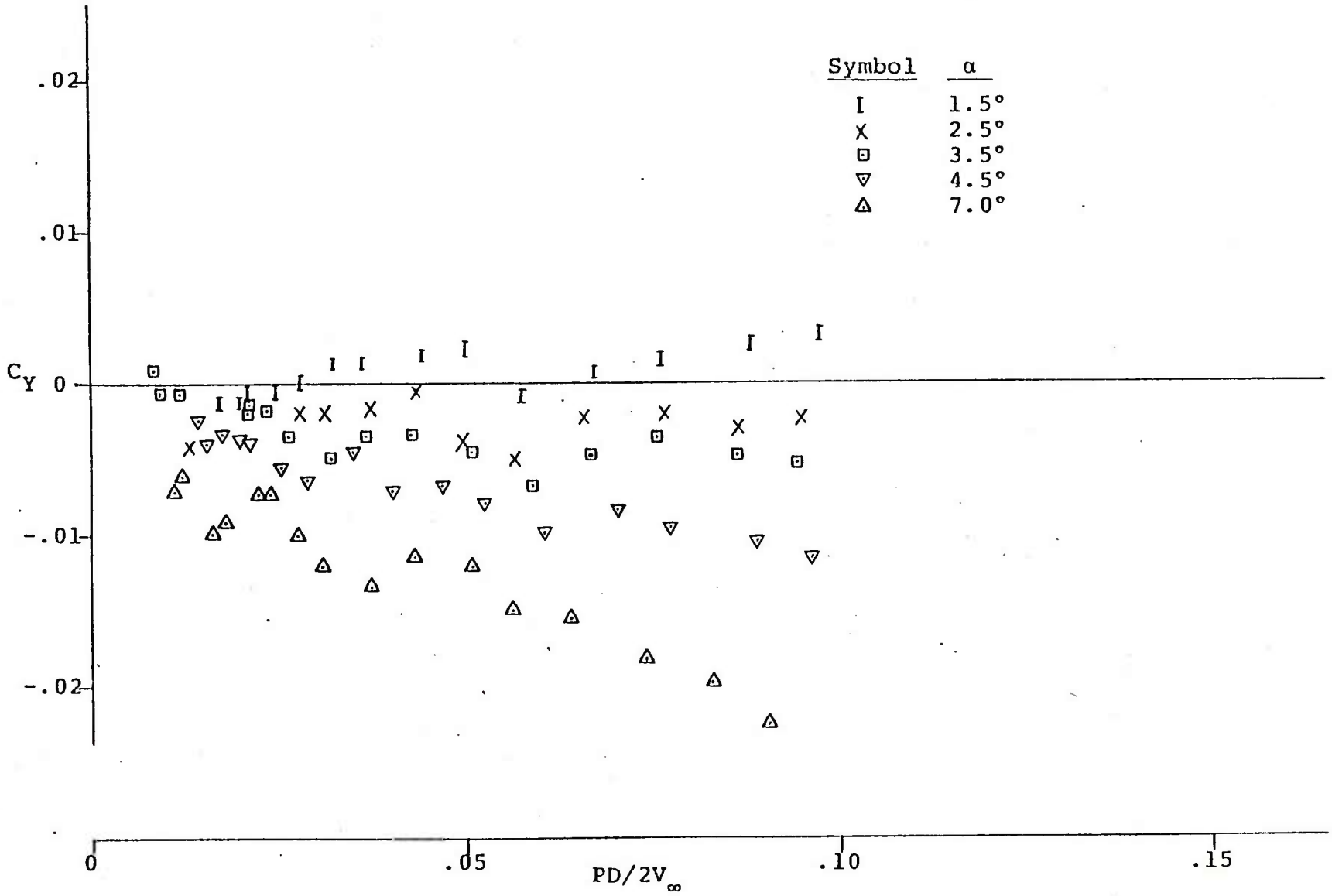

Figure 14a. C_Y vs. $PD/2V_\infty$ at $Re_L = .77 \times 10^6$ with Artificial Transition

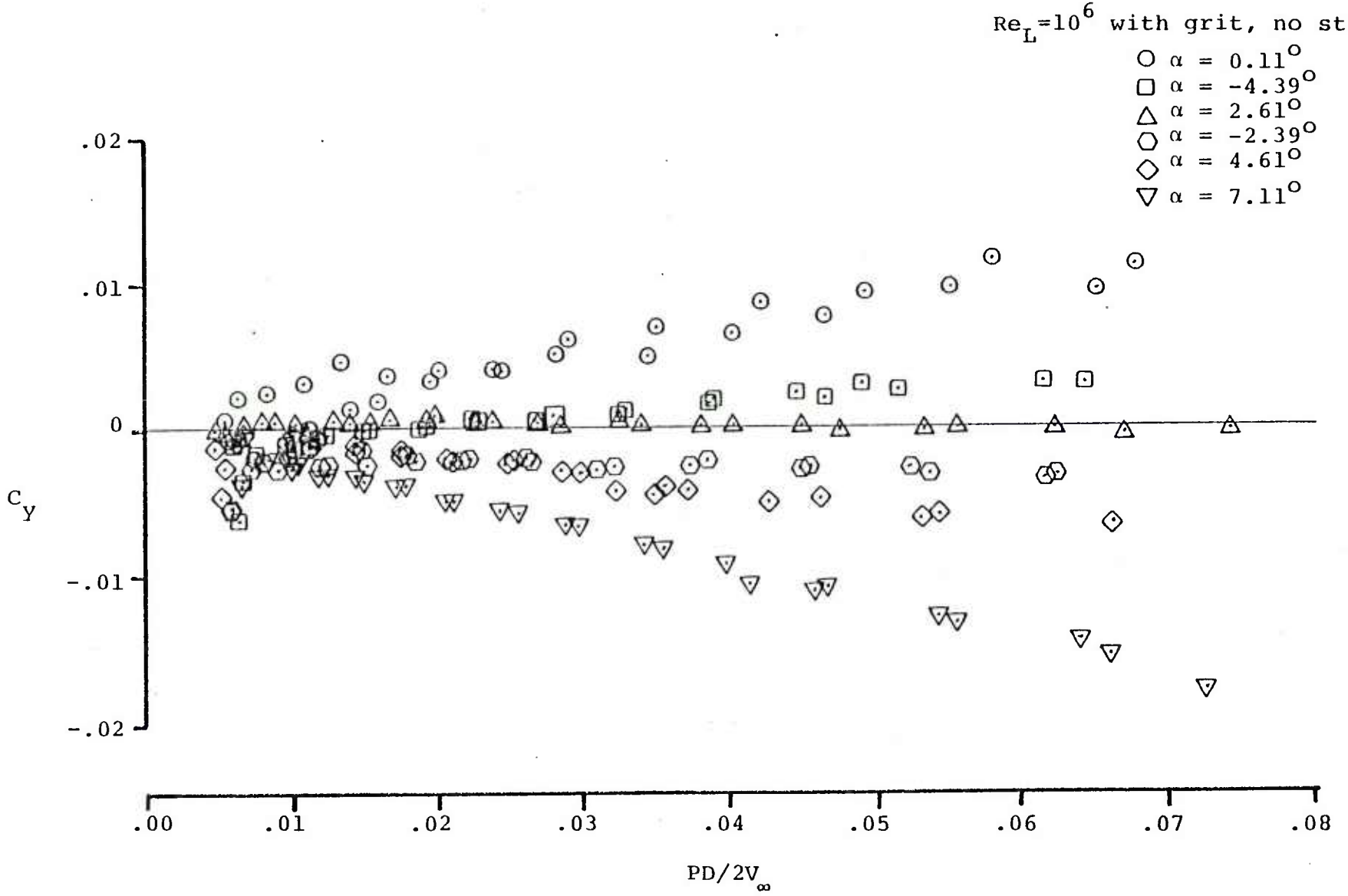

Figure 14b. Magnus Side Force Coefficient at $Re_L=10^6$ with Artificial Transition

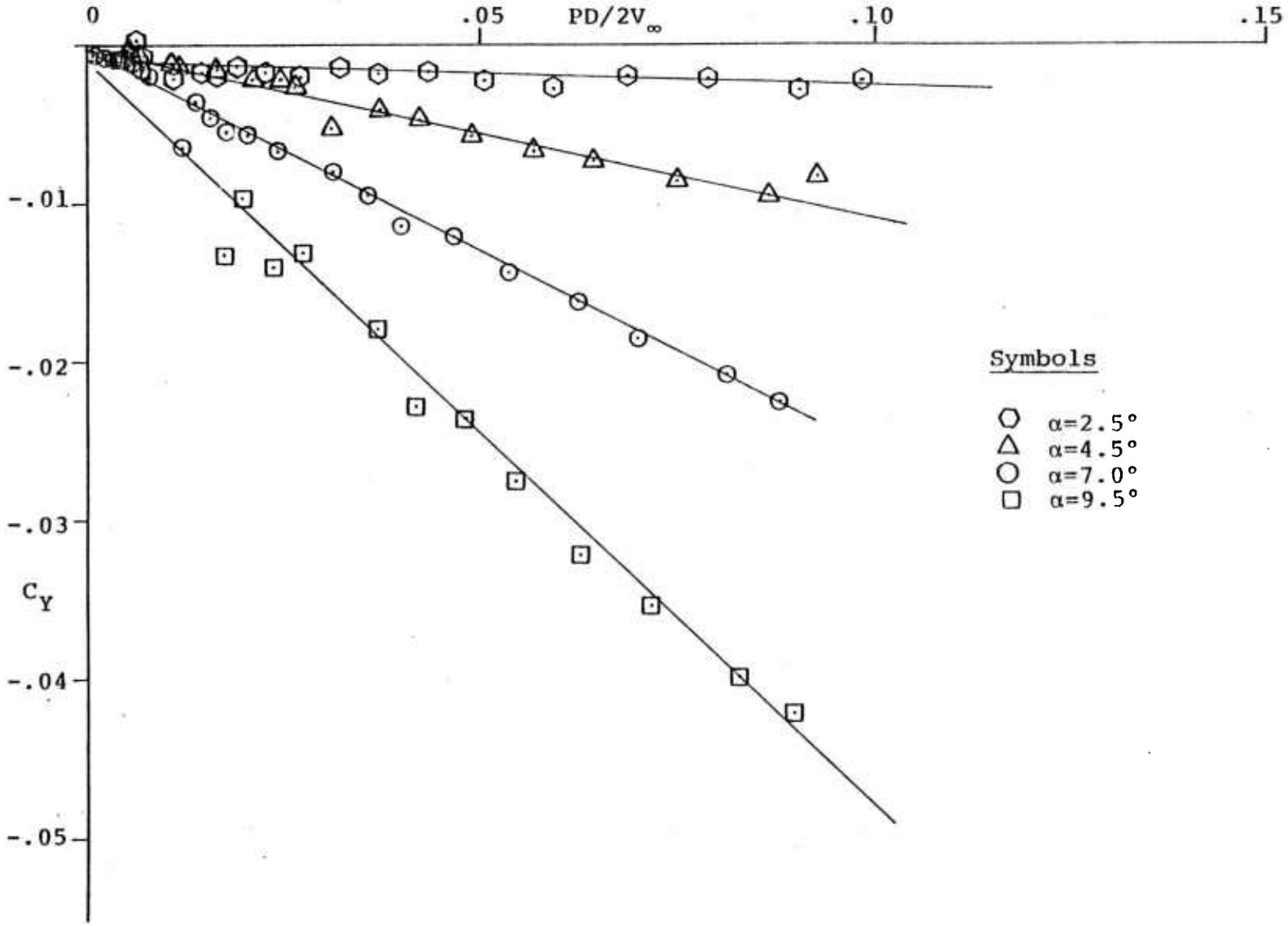

Figure 15. Effect of Grit and Sting C_Y vs. $PD/2V_\infty$; at $Re_L = .77 \times 10^6$

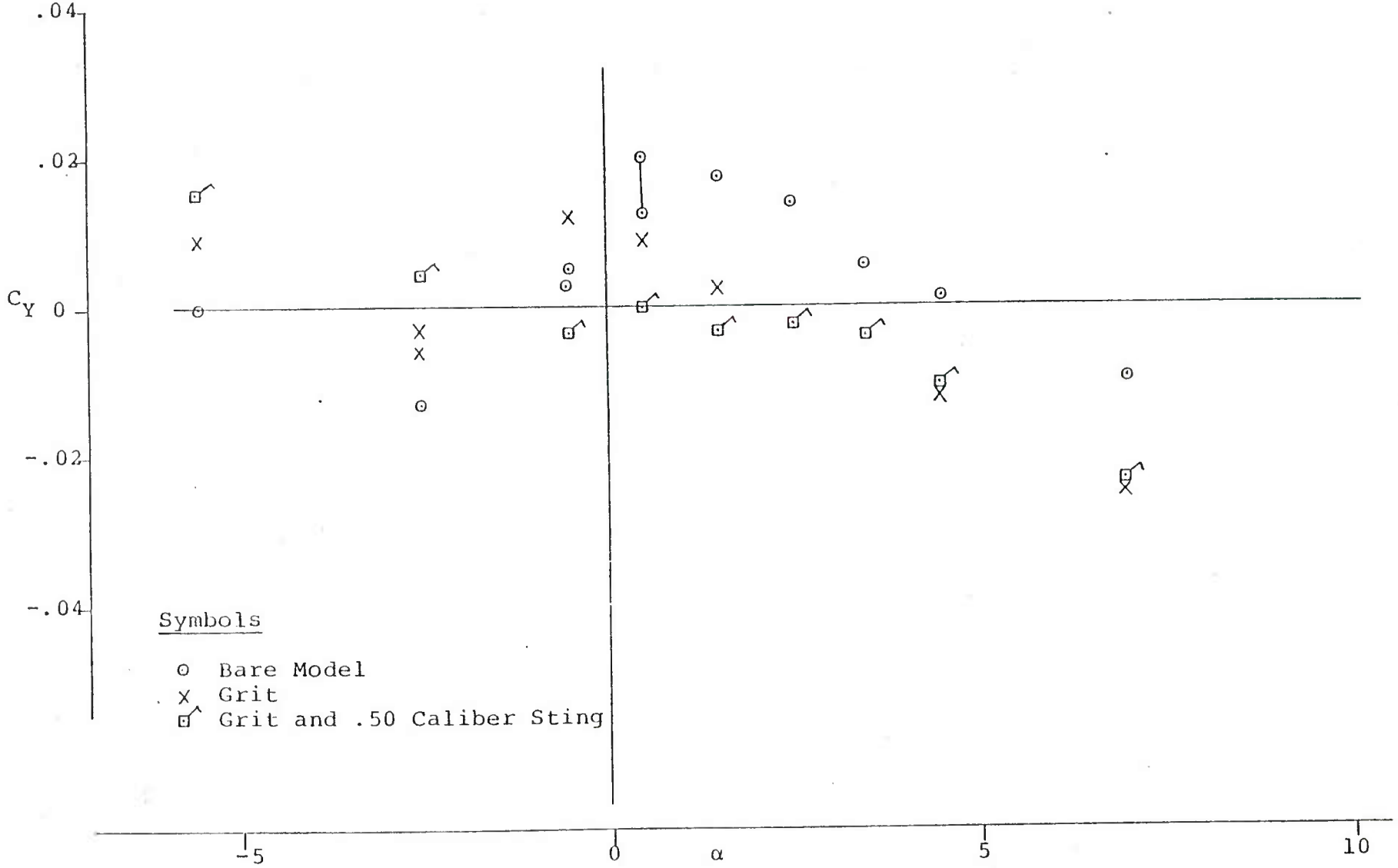

Figure 16. Grit Effect C_Y vs. α at $PD/2V_\infty = 0.1$ at $Re_L = .77 \times 10^6$

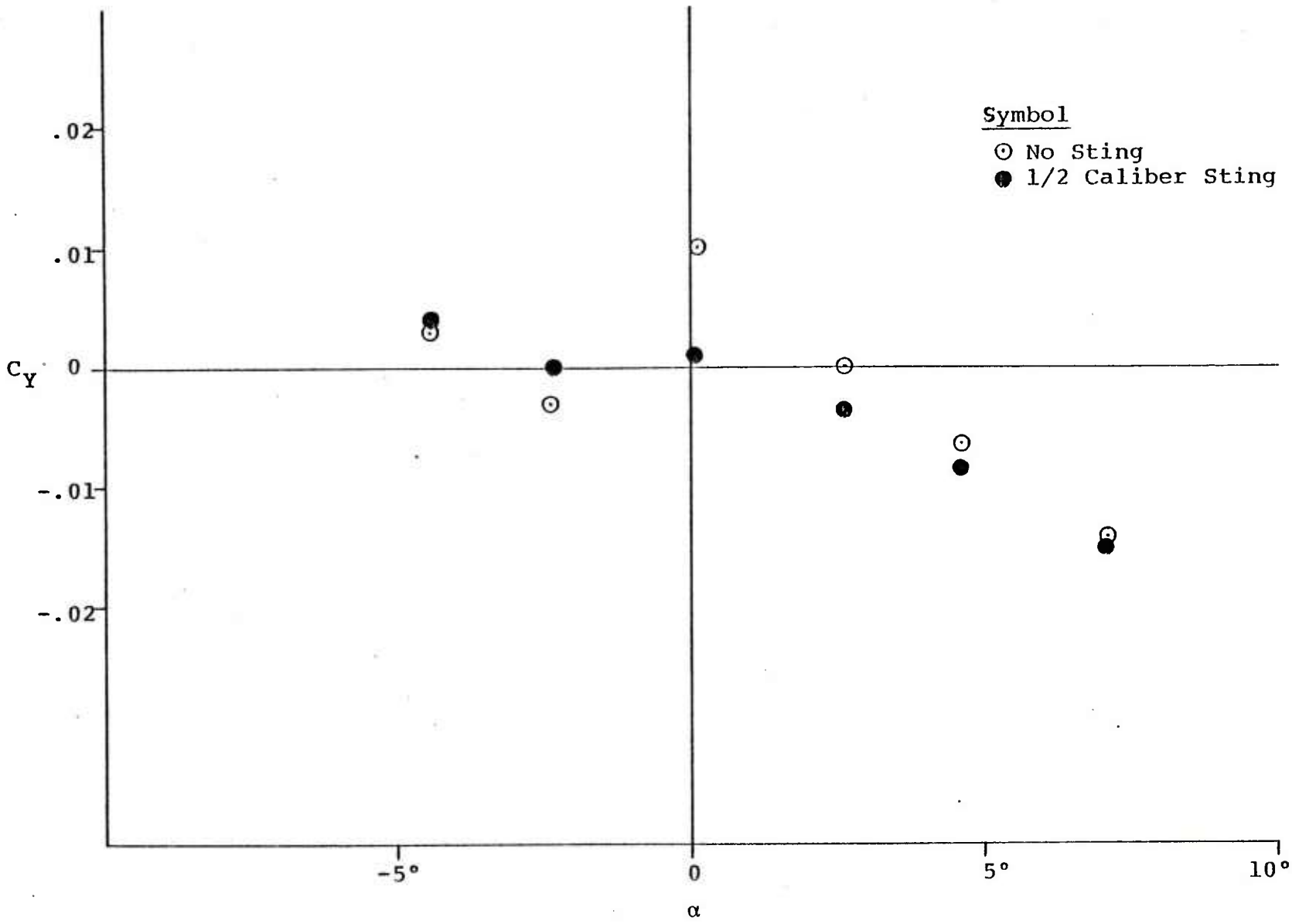

Figure 17a. C_Y vs. α for a Gritted Model at $PD/2V_\infty$ = .06 at $Re_L = 1.03 \times 10^6$

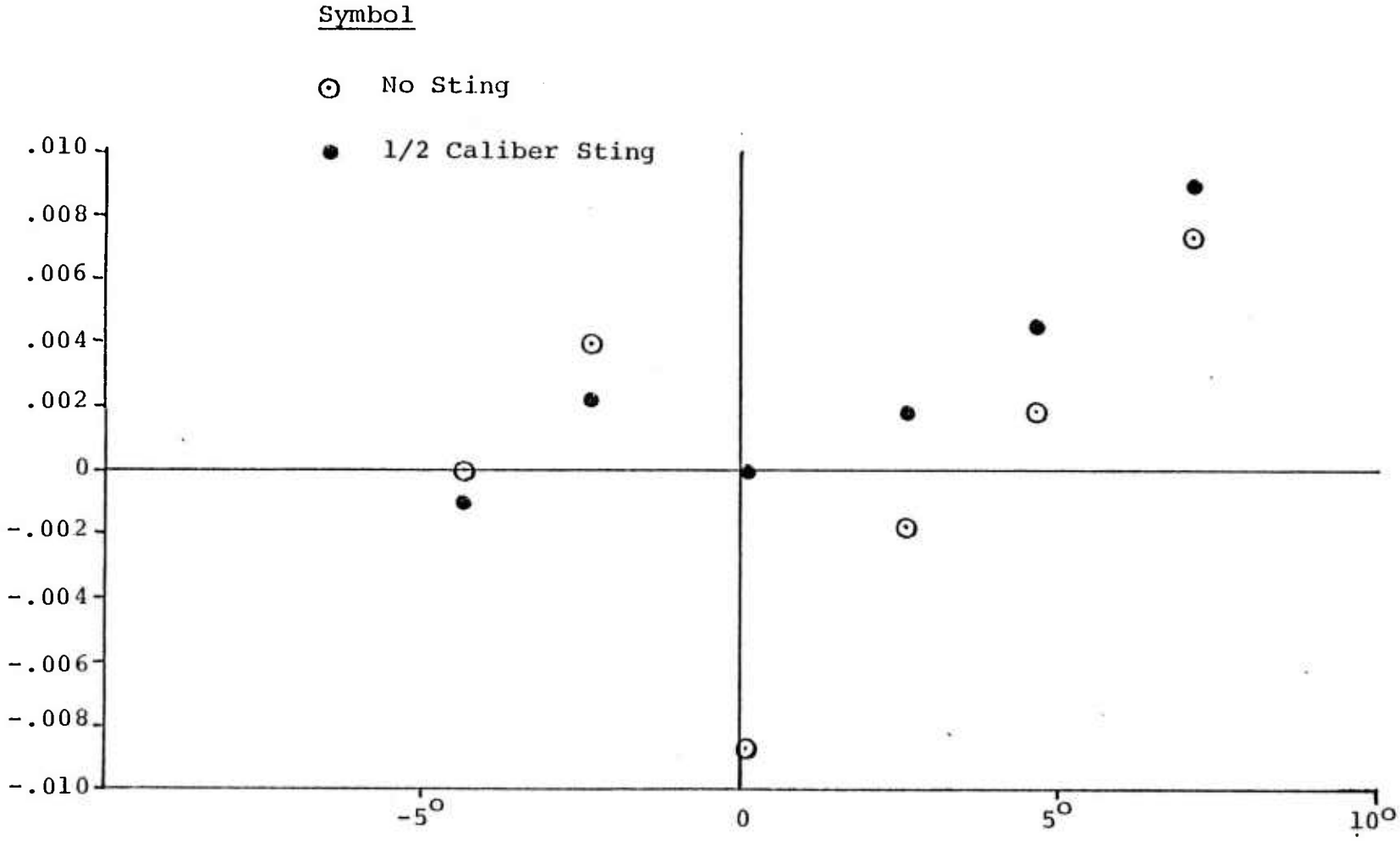

Figure 17b. C_N vs. α for a Gritted Model at $PD/2V_\infty$ = .06 at $Re_L = 1.03 \times 10^6$

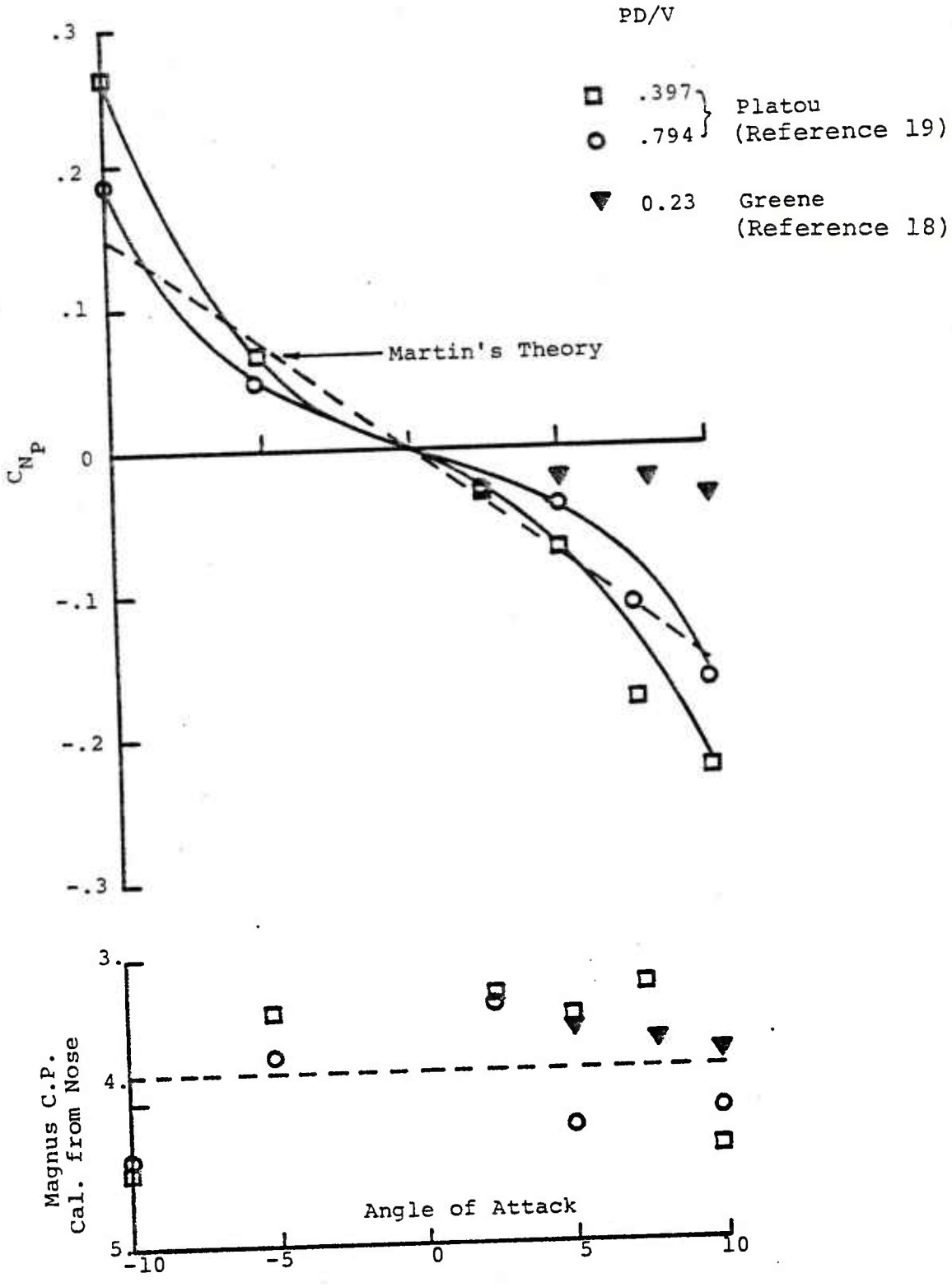

Figure 18. The Magnus Force after Platou (Reference 19)

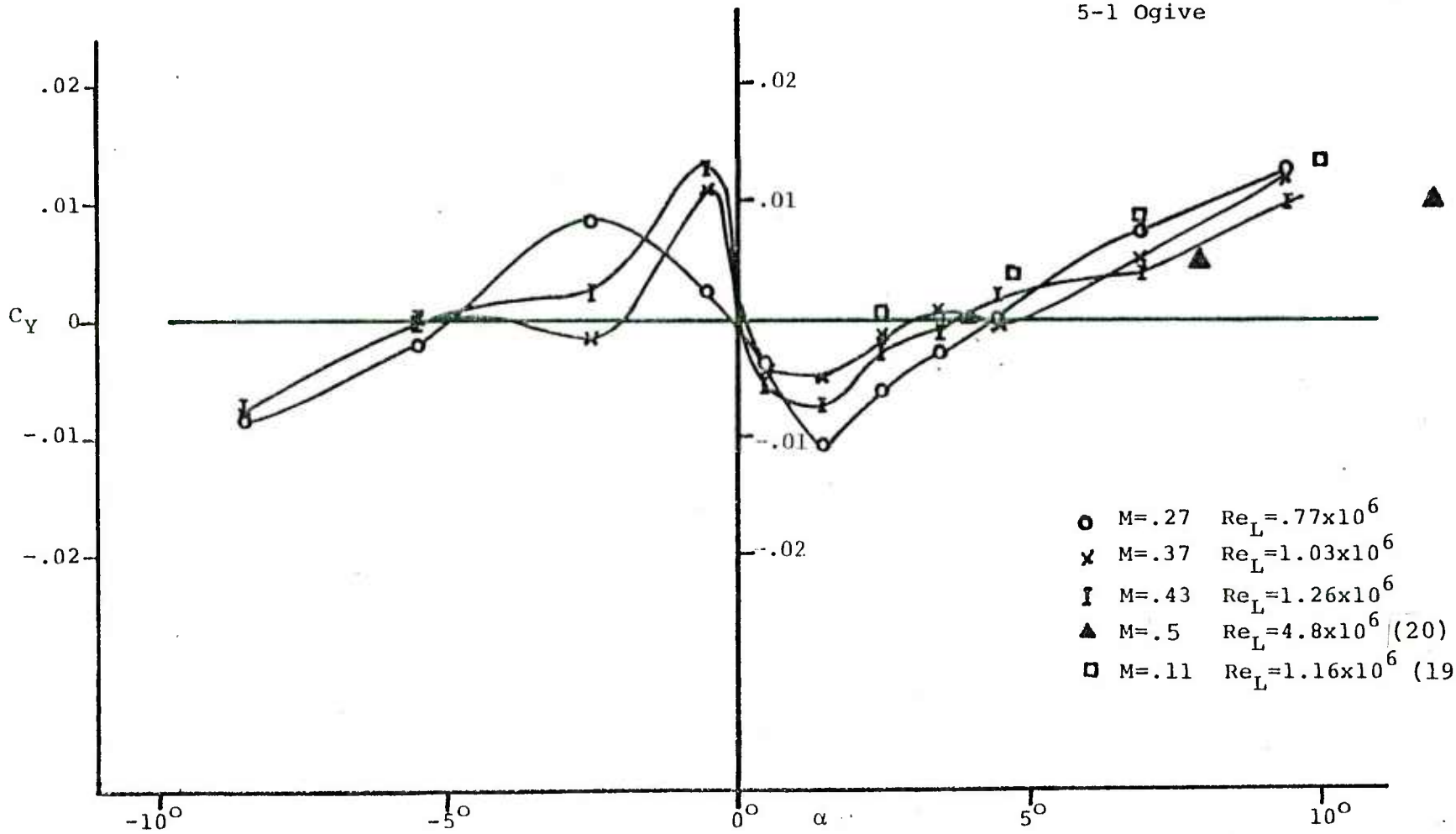

Figure 19. Side Force Coefficient vs. α at $PD/2V_\infty$ = .0450

Figure 20. Contour Plot of Magnus Force Coefficient for 2-dimensional Cylinder Cross Plotted from Swanson (5)

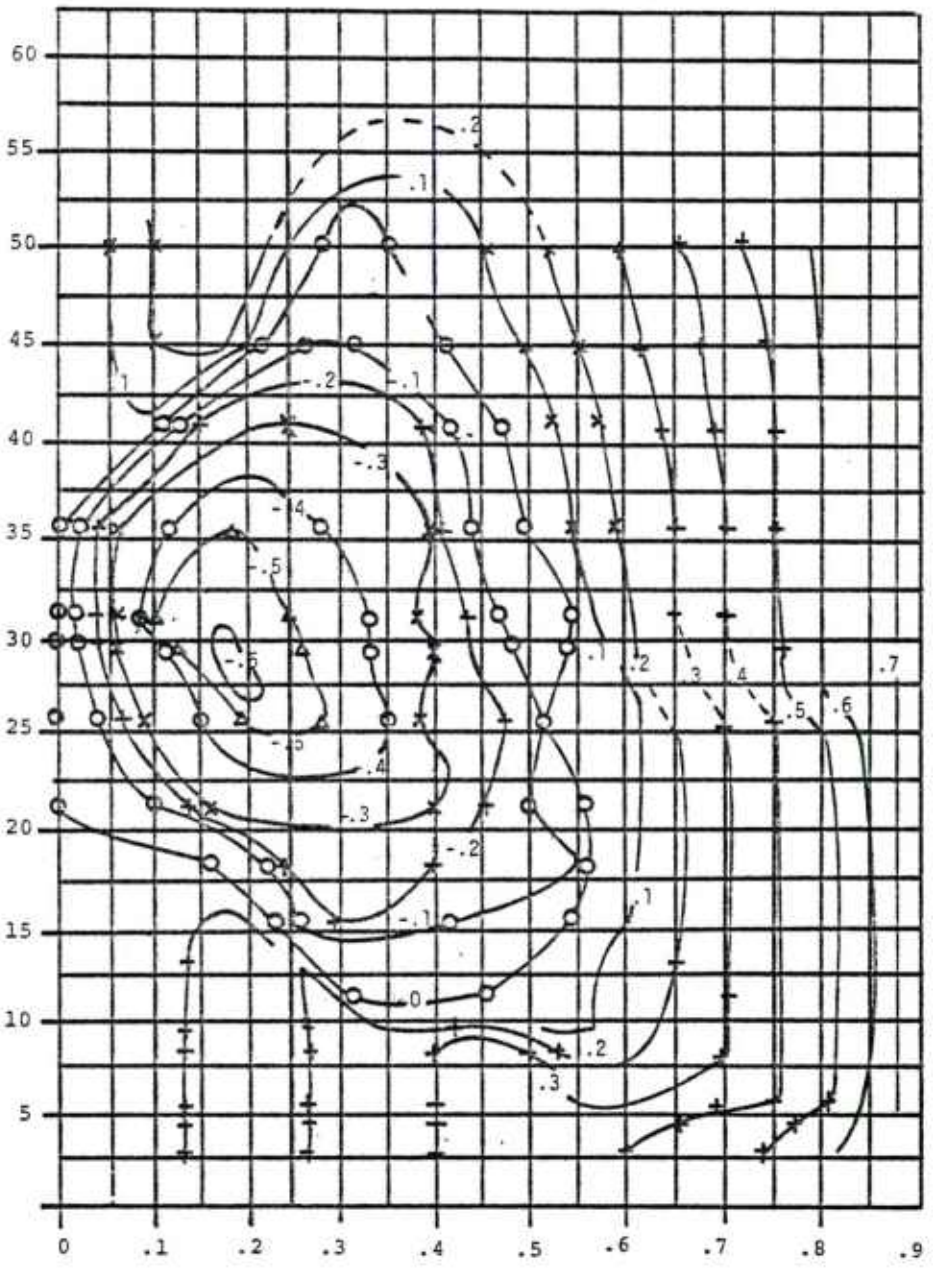

TEST MATRIX - 5:1 Ogive Run Numbers

Series	A		B		C		D*	E		F		G	
α	No Sting	No Trip	Large Sting	No Trip	Small Sting	No Trip		No Sting	Grit	Large Sting	Grit	No Sting	Ring Trip
-5.5	11		19	20	6	7		18	19	18	19	21	
-2.5	10	12	13	14	5	8		16	17	15	17	17	18
0.5	001	009	1	11	1	9		13	15	1	2	1 20	2 19
0.5	002	016	2	12	2	10		1 2	14	3	4	3	4
1.5	003	013	3	10	3	11		3 4	13	5	6	5	6
2.5	004	005 017	4	9	4	12		5	6	7	8	7	8
3.5	006	014	5	8	14	15		7	8	9	10	9	10
4.5	7	15	6	7	16	17		9	10	11	12	11	12
7.0	8		15	16	18	19		11	12	13	14	13	14
9.5			17 21	22	20	21				21	22	15	16

*D was static, C_D vs. Re_L test

Appendix A

ABBREVIATED RUN SCHEDULE

5:1 Ogive Test

Run Number	Date	Re_ℓ	Spinning	Sting	Boundary Layer Trip	Comments
5-001-034	12/72	7×10^5	Yes	No	No	None
5-035-056	12/72	10×10^5	Yes	No	No	None
5-057-086	12/72	30×10^5	Yes	No	No	None
Calibration	1/73	-	No	No	-	None
A	8/73	7×10^5	Yes	No	No	None
B	8/73	7×10^5	Yes	Large	No	None
C	8/73	7×10^5	Yes	Small	No	None
D	8/73	7×10^5	No	No	Grit	Variable Grit Length
E	8/73	7×10^5	Yes	No	Grit	None
F	8/73	7×10^5	Yes	Large	Grit	None
G	8/73	7×10^5	Yes	No	Trip Ring	None
Calibration	11/73	7×10^5	No	No	-	None
H	11/73	Varied	No	No	No	Transition
J	11/73	Varied	No	No	No	Studies
K	11/73	Varied	No	No	No	C_{D_o} vs Re
L	11/73	Varied	No	No	No	C_{D_o} vs Re
M	11/73	Varied	No	No	No	C_{D_o} vs Re
N	11/73	Varied	No	No	No	C_{D_o} vs Re
P	11/73	Varied	No	No	Grit	C_{D_o} vs Re
Q	11/73	7×10^5	No	Large	No	2 Caliber Long Sting
R	3/74	10×10^5	No	Large	No	2 Caliber Long Sting
S	3/74	30×10^5	No	Large	No	2 Caliber Long Sting
T	3/74	7×10^5	No	No	No	None
U	3/74	10×10^5	No	No	No	None
V	3/74	30×10^5	No	No	No	None
W	4/74	10×10^5	Yes	No	Grit	None
X	4/74	10×10^5	Yes	Large	Grit	None
Y	4/74	10×10^5	No	No	Grit	None
Z	4/74	10×10^5	No	Large	Grit	None
Calibration	4/74	10×10^5	No	-	-	None

Appendix B. NOTATION

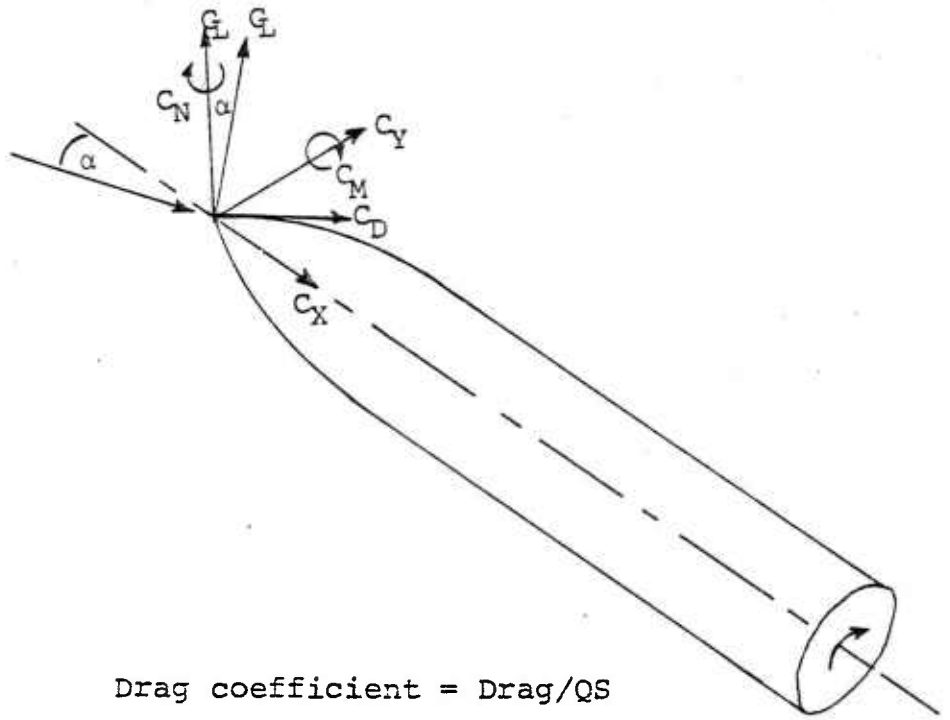

C_D	Drag coefficient = Drag/QS
C_L	Lift coefficient = Lift/QS
C_M	Pitching moment coefficient = pitching moment/QSL
C_{M_α}	Pitching moment slope
C_N	Magnus yawing moment coefficient = yawing moment/QSL*
C_{N_P}	Linear Magnus moment coefficient = $C_N/(PD/2V_\infty)$
C_x	Axial force coefficient
C_Y	Magnus side force coefficient = side force/QS*
C_{Y_P}	Linear Magnus force coefficient = $C_Y/(PD/2V_\infty)$
C_Z	Normal force coefficient
C_{Z_α}	Normal force coefficient slope
X_{cp}, CP	Center of pressure location diameters from the nose

D	Model diameter
L	Model length
M	Mach number
P	Spin rate - radians per second
Q	Dynamic pressure
Re_L	Reynolds number based on model length
Re_c	Cross flow Reynolds number
r	Body radius or radial coordinate
S	Model base area
u_x) u_x) u_θ)	Boundary layer velocity components
u_∞	Velocity of boundary layer edge
V_∞	Freestream velocity
x	Axial position
α	Angle of attack
Δ	Standard deviation
δ^*	Boundary layer displacement thickness
θ	Aximuthal coordinate

*No spin tare subtracted.

DISTRIBUTION LIST

No. of Copies	Organization
12	Commander Defense Documentation Center ATTN: DDC-TCA Cameron Station Alexandria, VA 22333
1	Commander US Army Materiel Development and Readiness Command ATTN: DRCDMA-ST 5001 Eisenhower Avenue Alexandria, VA 22333
1	Commander US Army Aviation Systems Command ATTN: DRSAV-E 12th and Spruce Streets St. Louis, MO 63166
1	Director US Army Air Mobility Research and Development Laboratory Ames Research Center Moffett Field, CA 94035
1	Commander US Army Electronics Command ATTN: DRSEL-RD Fort Monmouth, NJ 07703
3	Commander US Army Missile Command ATTN: DRSMI-R DRSMI-RDK Mr. R. Deep Mr. R. Becht Redstone Arsenal, AL 35809
1	Commander US Army Tank Automotive Development Command ATTN: DRDTA-RWL Warren, MI 48090
2	Commander US Army Mobility Equipment Research & Development Command ATTN: Tech Docu Cen, Bldg. 315 DRSME-RZT Fort Belvoir, VA 22060
1	Commander US Army Armament Command Rock Island, IL 61202
2	Commander US Army Frankford Arsenal ATTN: Mr. Spencer Hirschman Mr. John Sikra Bridge and Tacony Streets Philadelphia, PA 19137
5	Commander US Army Picatinny Arsenal ATTN: SARPA-AD Mr. S. Wasserman SARPA-FR-S-A Mr. D. Mertz Mr. E. Falkowski Mr. A. Loeb Mr. H. Hudgins Dover, NJ 07801
1	Commander US Army Jefferson Proving Ground ATTN: STEJP-TD-D Madison, IN 47250
1	Commander US Army Harry Diamond Labs ATTN: DRXDO-TI 2800 Powder Mill Road Adelphi, MD 20783
1	Commander US Army Natick Research and Development Center ATTN: DRXRE, Dr. D. Sieling Natick, MA 01762

DISTRIBUTION LIST

No. of Copies	Organization
1	Director US Army TRADOC Systems Analysis Activity ATTN: ATAA-SA White Sands Missile Range NM 88002
1	Commander US Army Research Office ATTN: Dr. Robert Singleton P. O. Box 12211 Research Triangle Park NC 27709
3	Commander US Naval Air Systems Command ATTN: AIR-604 Washington, DC 20360
2	Commander David W. Taylor Naval Ship Research & Development Ctr ATTN: Dr. S. de Los Santos Mr. Stanley Gottlieb Bethesda, MD 20084
1	Commander US Naval Surface Weapons Center ATTN: Dr. T. Clare, Code DK20 Dahlgren, VA 22448
2	Commander US Naval Surface Weapons Center ATTN: Code 312, S. Hastings Code 312, F. Regan Silver Spring, MD 20910
1	Commander US Naval Weapons Center ATTN: Code 5115 Dr. A. Charters China Lake, CA 93555
1	AFATL (DLDL) Eglin AFB, FL 32542
2	Director National Aeronautics and Space Administration Langley Research Center ATTN: Mr. Richmond P. Boyden Room 119, MS 404A Dr. Robert A. Kilgore Room 122, MS 404A Hampton, VA 23665
1	Director Jet Propulsion Laboratory ATTN: Mr. B. Dayman 4800 Oak Grove Drive Pasadena, CA 91103
1	Calspan Corporation ATTN: Mr. J. Andes, Head Transonic Tunnel Dept P. O. Box 235 Buffalo, NY 14221
1	Honeywell, Inc. ATTN: Mr. George Stilley 600 Second Street, N Hopkins, MN 55343
1	Sandia Laboratories ATTN: Division No. 9322 Mr. Warren Curry P. O. Box 5800 Albuquerque, NM 87115
2	Massachusetts Institute of Technology ATTN: Prof. E. Covert Prof. C. Haldeman 77 Massachusetts Avenue Cambridge, MA 02139

DISTRIBUTION LIST

No. of Copies	Organization
1	MIT/Lincoln Laboratories ATTN: Dr. Milan Vlajinac Mail Stop D-382 P. O. Box 73 Lexington, MA 02173
1	Rutgers University Mechanical, Industrial and Aerospace Engineering Department ATTN: Dr. Robert H. Page New Brunswick, NJ 08903
1	University of Virginia Department of Aerospace Engineering and Engineering Physics ATTN: Prof. I. Jacobson Charlottesville, VA 22904

Aberdeen Proving Ground

Marine Corps Ln Ofc
Dir, USAMSAA
Cdr, USAEA
ATTN: SAREA-DE-W
Mr. A. Flatau
Mr. M. Miller
Mr. J. Huerta